Dynamics of Finite-Size Particles in Chaotic Fluid Flows

Julyan H.E. Cartwright, Ulrike Feudel, György Károlyi, Alessandro de Moura, Oreste Piro, and Tamás Tél

Abstract We review recent advances on the dynamics of finite-size particles advected by chaotic fluid flows, focusing on the phenomena caused by the inertia of finite-size particles which have no counterpart in traditionally studied passive tracers. Particle inertia enlarges the phase space and makes the advection dynamics much richer than the passive tracer dynamics, because particles' trajectories can diverge from the trajectories of fluid parcels. We cover both confined and open flow regimes, and we also discuss the dynamics of interacting particles, which can undergo fragmentation and coagulation.

1 Introduction and Overview

A correct formulation of the problem of the motion of finite-size particles in fluid flows has presented difficult challenges for generations of fluid dynamicists. Although in principle this problem is "just" another application of the Navier–Stokes equation, with moving boundary conditions, a direct solution of the fluid dynamical equations is not only very difficult, but also not very illuminating. So from the nineteenth century onwards efforts were made to find the appropriate approximations which allow one to write the equations of motion of small rigid particles in a given flow in the form of ordinary differential equations, regarding the flow's velocity field as given. Some very subtle issues are involved in making the right kinds of approximations and assumptions in a self-consistent way, and a number of incorrect results appeared in the early literature. The issue was finally resolved when Maxey and Riley [1] wrote down the equations of motion for a small spherical rigid particle advected by a (smooth) flow and Auton et al. [2], following Taylor's work [3], corrected the form of the added-mass term.

A. de Moura (✉)
Institute of Complex Systems and Mathematical Biology, University of Aberdeen, King's College, Meston Building, AB24 3UE Aberdeen, United Kingdom
e-mail: a.moura@abdn.ac.uk

M. Thiel et al. (eds.), *Nonlinear Dynamics and Chaos: Advances and Perspectives,* Understanding Complex Systems, DOI 10.1007/978-3-642-04629-2_4,

The Maxey-Riley equations allow the global dynamics of a single advected finite-size particle to be investigated with the techniques of dynamical systems theory. The dynamics of advected particles in fluid flows have been a favourite subject of investigation of chaos and related complex dynamical regimes since the pioneering work of Aref [4], but all the early works assumed that the particles' size and their inertia could be neglected – the *passive tracer* assumption. Finite size results in inertia, which introduces a new richness to the dynamics, since finite-size particles are no longer enslaved to the motion of the flow surrounding them – they have their own dynamics, distinct from that of the fluid. A whole new world of challenges and possibilities opens up to dynamicists once finite size and inertia are considered. This gives this subject a great importance from the theoretical point of view alone; not to mention its practical importance: polluting particles suspended in the atmosphere and plankton organisms floating in the ocean are just a few of the systems whose understanding involves the theory of the dynamics of finite-size particles in complex flows.

This chapter presents an overview of the subject of the dynamics of finite-size particles in chaotic flows, focusing on a few chosen topics of current research. The choice of topics reflects the authors' own research interests; we make no apologies for that: we in no way claim this to be an exhaustive review on this area. But we do think the topics we cover here give the reader a good idea of what is going on in this exciting area of research.

We first introduce the Maxey-Riley equation in Sect. 2. Its assumptions and range of validity are discussed, as well as some of its basic consequences; but we do not show the derivations. The dynamics of finite-size particles can often be understood by using the simpler dynamics of passive tracers as a starting point. In Sect. 3 we discuss the chaotic advection of non-inertial tracers, and also introduce some of the flows which will be used as examples in later sections.

The dynamics of non-interacting finite-size particles is the subject of Sects. 4 and 5. Section 4 deals with confined flows, whereas Sect. 5 focuses on open flows. These two kinds of flow have very different long-time behaviours, which lead to quite distinct particle dynamics. In these sections, we focus especially on the new phenomena caused by the particles' inertia, which are not present in the case of passive tracers. The challenging and very important topic of interacting finite-size particles is covered by Sect. 6, which reviews recent results on the processes of fragmentation and coagulation of finite-size particles. Finally, in Sect. 7, we make some remarks on the future directions of this research area.

2 Motion of Finite-Size Particles in Fluid Flows

When studying the motion of particles advected by fluid flows, it is commonly assumed that one can consider the particles as *passive tracers*, with negligible mass and size. This amounts to neglecting the particles' inertia, and assuming that they take on the velocity of the surrounding fluid, instantaneously adapting to any changes in the fluid velocity. If $\mathbf{u}$ is the (possibly time-dependent) fluid's velocity

field, and denoting by $\mathbf{r}(t)$ the position of a particle, the passive tracer assumption implies that $\mathbf{r}$ satisfies the differential equation:

$$\dot{\mathbf{r}}(t) = \mathbf{u}(\mathbf{r}(t),t). \tag{1}$$

The passive tracer assumption is extensively used in fluid dynamics [5, 6], and it is a good approximation in a number of cases. There are many situations, however, where it does not apply, and we need to take into account the fact that particles have finite sizes and masses (for reviews see [7–9]). Finite-size particles are not able to adjust their velocities instantaneously to that of the fluid, and in addition their density may be different from that of the fluid. Therefore, in general the particle velocity differs from the fluid velocity. This means that the dynamics of finite-size particles is far richer and more complex than that of passive tracers.

2.1 The Maxey-Riley Equation

In order to study the dynamics of finite-size particles advected by chaotic flows, we need to have a simple formulation of the equations of motion of the advected particles. The problem is that finite-size particles are actually extended objects with their own boundaries. The rigorous way to analyse their dynamics would involve solving the Navier–Stokes equation for moving boundaries, with all the complications this implies. The partial differential equations resulting from this approach would be very difficult to solve and analyse; and as dynamicists, we would like to have the particle's motion described by ordinary differential equations, similar to Eq. (1). Fortunately, an approximate differential equation for the motion of small spherical particles in flows may be written down [1, 2]. If a particle has radius a and mass m_p, its motion is given to a good approximation by the *Maxey-Riley equation*:

$$\begin{aligned} m_p\dot{\mathbf{v}} = m_f\frac{D}{Dt}\mathbf{u}(\mathbf{r}(t),t) - \frac{1}{2}m_f\left(\dot{\mathbf{v}} - \frac{D}{Dt}\left[\mathbf{u}(\mathbf{r}(t),t) + \frac{1}{10}a^2\nabla^2\mathbf{u}(\mathbf{r}(t),t)\right]\right) \\ -6\pi a\rho_f\nu\mathbf{q}(t) + (m_p - m_f)\mathbf{g} - 6\pi a^2\rho_f\nu\int_0^t d\tau\,\frac{d\mathbf{q}(\tau)/d\tau}{\sqrt{\pi\nu(t-\tau)}}, \end{aligned} \tag{2}$$

where

$$\mathbf{q}(t) \equiv \mathbf{v}(t) - \mathbf{u}(\mathbf{r}(t),t) - \frac{1}{6}a^2\nabla^2\mathbf{u}.$$

Here $\mathbf{r}(t)$ and $\mathbf{v}(t) \equiv d\mathbf{r}(t)/dt$ are the position and velocity of the particle, respectively, and $\mathbf{u}(\mathbf{r},t)$ is the undisturbed flow field at the location of the particle. m_f denotes the mass of the fluid displaced by the particle, and ν is the kinematic viscosity of the fluid of density ρ_f; $\mathbf{g}$ is the gravitational acceleration.

The derivative

$$\frac{D\mathbf{u}}{Dt} = \frac{\partial\mathbf{u}}{\partial t} + (\mathbf{u}\cdot\nabla)\mathbf{u} \tag{3}$$

is the total hydrodynamical derivative, taken along the path of a fluid element, whereas

$$\frac{d\mathbf{u}}{dt} = \frac{\partial \mathbf{u}}{\partial t} + (\mathbf{v} \cdot \nabla)\mathbf{u} \tag{4}$$

is taken along the particle's trajectory.

The first term on the right-hand side is the acceleration of the fluid element in position $\mathbf{r}(t)$ at time t and represents the force exerted on the particle by the undisturbed fluid. The second term represents the *added-mass effect*, which accounts for the fact that when the particle moves relative to the fluid, it displaces a certain amount of fluid with it; the result is that the particle behaves as if it had additional mass. The third and fourth terms represent the Stokes drag caused by the fluid's viscosity and the buoyancy force, respectively. The integral is called the *Basset-Boussinesq history term*, and arises from the fact that the vorticity diffuses away from the particle due to viscosity [10, 11]. The terms involving the factor $a^2\nabla^2\mathbf{u}$ are the so-called *Faxén corrections* [94], and they account for the spatial variation of the flow field across the particle.

Equation (2) is valid for small particles at low particle Reynolds numbers Re_p. This Reynolds number is calculated by using the particle size as the length scale, and the relative velocity between particle and neighbouring fluid as the velocity scale: $\mathrm{Re}_p = a|\mathbf{v} - \mathbf{u}|/\nu$. This implies that for Eq. (2) to be a valid approximation, the initial velocity difference between particle and fluid must be small [1]. Another condition is that the velocity difference across the particle – more precisely, the shear Reynolds number $\mathrm{Re}_\Gamma = a^2\Gamma/\nu \ll 1$, where Γ is the typical velocity gradient in the flow – must be small [1].

If the typical length over which the velocity field changes appreciably is much larger than the particle radius a, the Faxén corrections can be neglected. Since the Basset-Boussinesq history term also describes the effect of viscosity (just like the Stokes drag), in a minimal model it can also be neglected. These approximations simplify tremendously the equations of motion. The history term would be especially problematic to analyse, since it depends on the entire past history of the particle, and it means the dynamics described by Eq. (2) has an infinite-dimensional phase-space. By neglecting it, Eq. (2) is an ordinary differential equation (and not an integro-differential equation), which can be studied with the techniques presently available to dynamical systems theory.

Using these approximations, we redefine the variables by

$$\mathbf{r} \to \mathbf{r}L, \quad \mathbf{v} \to \mathbf{v}U, \quad \mathbf{u} \to \mathbf{u}U, \quad t \to \frac{L}{U}t,$$

where L and U are the typical length and velocity scales of the flow. The new variables are all dimensionless. In these new variables, we get the following dimensionless equation of motion:

$$\ddot{\mathbf{r}}(t) = \frac{1}{\mathrm{St}}\left(\mathbf{u}(\mathbf{r}(t),t) - \dot{\mathbf{r}}(t) + W\mathbf{n}\right) + \frac{3}{2}R\frac{D}{Dt}\mathbf{u}(\mathbf{r}(t),t), \tag{5}$$

where **n** is a vertical unit vector pointing downwards, and the dimensionless parameters are

$$\mathrm{St}^{-1} = \frac{6\pi a \rho_f \nu L}{\left(m_p + \frac{1}{2} m_f\right) U}, \quad R = \frac{m_f}{m_p + \frac{1}{2} m_f}, \quad W = \frac{m_p - m_f}{6\pi a \nu \rho_f U} g, \tag{6}$$

with $g = |\mathbf{g}|$. The parameter St measures the damping intensity and is called the *Stokes number*, the dimensionless decay time in the velocity difference between particle and fluid due to the Stokes drag. The limit of $\mathrm{St} \to 0$ corresponds to the case of point particles with no inertia (since m_f and m_p are proportional to a^3). It is in this limit that the passive tracer equation (1) holds. R is the mass ratio parameter. $R < \frac{2}{3}$ corresponds to aerosols (particles heavier than the fluid), and $R > \frac{2}{3}$ corresponds to bubbles (particles lighter than the fluid). W is the scaled particle settling velocity for still fluid. Note that W/St is the dimensionless buoyancy force, which is independent of the particle size. Unless otherwise noted, we shall use Eq. (5) for the remainder of this work to describe the dynamics of finite-size particles.

2.2 General Features of the Dynamics of Finite-Size Particles

Finite-size particles have very different dynamics from that of passive tracers, which follow the same dynamics as fluid parcels. Mathematically, this is expressed by the fact that Eq. (5) is a second-order differential equation, compared with Eq. (1) which is of first order. An immediate consequence of this is that the finite-size dynamics given by Eq. (5) possesses a $2n$-dimensional phase-space, where n is the dimension of the configuration space. Thus, in a planar flow a finite-size particle is described by a dynamical system with four degrees of freedom. In contrast, for non-inertial particle dynamics the phase-space is two-dimensional.

Another difference is that the finite-size dynamics is dissipative, even in incompressible flows, and the phase-space volume contracts at the rate n/St, which is always positive. Contrast this to the non-inertial case, in which the phase-space volume coincides with the spatial volume, which renders the dynamics conservative for incompressible flows. The dissipative character of the finite-size dynamics raises the possibility of the existence of attractors in phase-space, which is not possible in the non-inertial case. This has crucial consequences for the global dynamics of particles in chaotic flows, as we shall see in later sections.

The density of an advected particle relative to the surrounding fluid plays a crucial role in its dynamics. This is incorporated in the parameter R in Eq. (5). Using a perturbative analysis valid in the limit of small particle sizes, Maxey has shown [12] that if particles have higher density than the fluid (aerosols, with $R < \frac{2}{3}$), they tend to move away from regions of high vorticity, such as the centres of eddies. This effect can be intuitively understood as the result of a centrifugal force acting on the particle and pushing it away from a highly-rotating region. Conversely, particles with lower density than the fluid (bubbles, with $R > \frac{2}{3}$) tend to move towards high-vorticity regions. So bubbles tend to agglomerate in the centres of vortices. These effects are totally absent in the non-inertial case.

3 Chaotic Advection of Passive Tracers

In order to understand properly the dynamics of finite-size particles in chaotic flows, we must first understand the simpler dynamics of passive tracers. In this section we review passive advection of particles from the viewpoint of dynamical-systems theory. In the approximation of passive advection, the particles are considered to be massless and of negligible size. They take on the velocity of the fluid flow instantaneously, and their motion is given by Eq. (1). The flows we shall consider here are typically laminar, i.e., the velocity field **u** is assumed to be smooth, although time-dependent. We briefly discuss the case of turbulent flows in the concluding Section.

3.1 Properties of Passive-Tracer Chaotic Advection

The velocity field of the fluid, described by the right-hand side of (1), is typically a non-linear function of the position and time. This implies that even if the flow itself is relatively simple and non-turbulent, the solutions of (1) can become chaotic, a phenomenon named chaotic advection by Aref [4]. This is an essential difference between the Eulerian description of fluid motion, which is concerned with the properties of the velocity field of the fluid, and the Lagrangian description, which is concerned with the trajectories of the fluid elements. It is argued in [13] that the advection in any flow with a fluid Reynolds number high enough to generate a time dependent velocity field around an obstacle displays chaos.

The stretching and folding action of the chaotic dynamics acting on a set of initial conditions in the phase space, which coincides with the configuration space, can be seen directly through the behaviour of a blob of dye injected into the fluid. As a

Fig. 1 Surface patterns downstream of the flow-through of a power plant. Loch Faskally, Scotland, photo taken by Gy. Károlyi. The scale is approximately 2 m

result, an initially compact blob of particles will trace out a complex filamentary structure; a real-world example is shown in Fig. 1. In most examples in the area of dynamical systems, these complex patterns are hidden in a high-dimensional abstract phase space; here they become visible to the naked eye, and can be photographed in experiments [14, 15].

We assume throughout this work that the fluid is incompressible. As a consequence, the motion of passively advected particles is volume preserving, hence the motion of passive tracers is similar to Hamiltonian dynamics, where the phase space volume is conserved during motion [16]. This property is unique to passively advected particles.

Advection in *two-dimensional* ($\mathbf{r} = (x,y)$, $\mathbf{u} = (u_x,u_y)$) and *incompressible* flows represents an important subclass of chaotic advection systems. Incompressibility implies that there exists a stream function $\Psi(x,y,t)$ so that the velocity components can be written as

$$u_x(x,y,t) = -\frac{\partial \Psi(x,y,t)}{\partial y}, \quad u_y(x,y,t) = \frac{\partial \Psi(x,y,t)}{\partial x}. \tag{7}$$

Substituting this into (1) we obtain the equation of motion for a particle advected in 2D in terms of the stream function:

$$\frac{dx}{dt} = -\frac{\partial \Psi(x,y,t)}{\partial y}, \quad \frac{dy}{dt} = \frac{\partial \Psi(x,y,t)}{\partial x}. \tag{8}$$

These equations have a clear Hamiltonian structure, variable x playing the role of the position, y playing the role of the conjugate momentum, and $\Psi(x,y,t)$ playing the role of the Hamiltonian function [17, 18].

If the flow is stationary, that is, the stream function Ψ does not depend explicitly on time, the particle trajectories coincide with the level curves of Ψ, called streamlines [17, 18]. From a dynamical point of view, passive advection in a stationary, incompressible 2D flow is a one-degree-of-freedom Hamiltonian system, which is always integrable. In most realistic situations, however, Ψ is not independent of time, in which case we have a one-degree-of-freedom system with a time-dependent Hamiltonian. Such driven systems typically exhibit chaotic motion [19, 20]: the advected particles move in an unpredictable way and display a great sensitivity to initial conditions. Even a very simple time dependence, for example periodicity, is enough to generate chaotic particle motion: no turbulence is necessary for complex particle trajectories. This phenomenon is often called *Lagrangian turbulence*, in contrast to the spatiotemporal complexity of a flow field, which is referred to as Eulerian turbulence.

Flows can be divided into two main classes: they can be either *open* or *closed*. A flow is closed if it is confined within a bounded domain. A flow is considered open if there is a net current flowing through the region of observation and if fluid elements cannot return there from the outflow region. A typical example of closed flow is mixing in a batch reactor without in- or outflow; an example of an open flow is the fluid motion in a channel or river in the presence of an

obstacle. In open flows, most trajectories are unbounded, and most particles escape the observation region in a finite time. In closed flows, the particles cannot escape the bounded region. Therefore chaotic behaviour, if it occurs, is persistent in closed flows. Such flows reveal structures commonly found in usual Hamiltonian systems, with chaotic regions coexisting with regular islands. Advected particles, if they start from an initial position in the chaotic region, roam the whole chaotic region, whereas particles within a regular island remain inside forever. The boundaries of these islands, formed by Kolmogorov-Arnold-Moser (KAM) tori, are impenetrable to outside particles. In the chaotic regions, particles initiated close to each other deviate exponentially along the unstable foliation of unstable fixed points. This unstable foliation is dense in the chaotic regions, and governs the stretching and folding of dye blobs. When stretching of a dye blob starts, a filamentary structure emerges, which becomes space-filling in the limit of long times. Thus, *persistent chaos* and *transient filamentary structures* are features found in closed flows.

The chaotic motion of passively advected particles in open flows takes a different form. Typical particles escape the observation region in finite time, but there is a fractal set of particle trajectories confined within a finite region, e.g. in the vicinity of the wake in a flow around an obstacle. These non-escaping orbits form a non-attracting chaotic set, a *chaotic saddle* [19, 20], which governs the motion of particles in its vicinity. This chaotic set, although it consists of unstable orbits and has measure zero, gives rise to extreme sensitivity of the dynamics to initial conditions. The stable manifold of the chaotic saddle separates the initial conditions leading to different final states of the particles (such as where they leave the region of observation). The unstable manifold of the chaotic saddle is traced out by the particles that spend long times in the vicinity of the saddle. Because the unstable manifold is a filamentary fractal, the pattern traced out by a blob of dye takes on a complex shape, shadowing the fractal structure of the unstable manifold. Advection thus leads to *transient chaos* owing to particles leaving the region of observation, and to *persistent filamentary structures* traced out by the advected particles.

In the following subsections some paradigmatic flows, both open and closed, are reviewed. These flows will be used later to illustrate the motion of finite-size particles.

3.2 The Convection and Cellular Flow Models

The convection flow is a simple two-dimensional incompressible flow representing vortices or roll cells with oscillating velocity magnitude. It was introduced by Chandrasekhar [21] as a solution to the Bénard problem and has been used since then in many studies involving active and passive particles [22, 23]. The flow is defined on a unit cell, but one may study the motion of finite-size particles on an infinite spatial domain using periodic boundary conditions. The convection flow is particularly interesting to investigate the principles of particle motion in the ocean and in the atmosphere since it contains both vortices (convection cells) and linear

uprising/sinking regions, and can hence be considered as an idealisation of realistic atmospheric and oceanic flows. The flow is given by the stream function

$$\psi(x,y,t) = [1 + B\sin(\omega t)]\frac{1}{k}\sin(kx)\sin(ky). \tag{9}$$

Here it is assumed that the characteristic velocity $U_0 = 1$ and the characteristic length scale of the flow $L = 1$, and we set $k = 2\pi$ accordingly. The parameters B and ω denote the amplitude and the frequency of the oscillation of the vortical velocity magnitude, respectively.

A special feature of the flow described by Eq. (9) it that the non-inertial advection dynamics remains nonchaotic even in the time-dependent case. In this flow chaotic advection can only be the consequence of finite-size effects.

To illustrate the flow field we show a snapshot of the velocity field in Fig. 2. This flow field with the parameters $B = 2.72$, $\omega = \pi$ is used later for all results concerning coagulation and fragmentation processes (cf. Sect. 6).

We also consider a slightly modified version of the convection flow, the cellular flow model. This is a two-dimensional incompressible flow representing a lattice of oscillating vortices or roll cells. The flow is defined by the stream function

$$\psi(x,y,t) = \frac{1}{k}\cos(kx + B\sin(\omega t))\cos(ky). \tag{10}$$

The flow is defined in the $x,y \in [-\pi/2,\pi/2]$ domain with periodic boundary conditions, and k is set to 1.

Let us first consider the simplest case where the time dependence is suppressed, by setting $B = 0$. Thence ψ is a constant of motion, which implies that real fluid elements follow trajectories that are level curves of ψ. This is illustrated in Fig. 3a. For $B \neq 0$, the equations of motion for fluid element or passive tracer are given by (7) and the trajectories differ from the streamlines. An example is shown in Fig. 3b, where the Poincaré section of the particle motion is illustrated. The positions of many particles are plotted at integer multiples of the flow period. Some of the

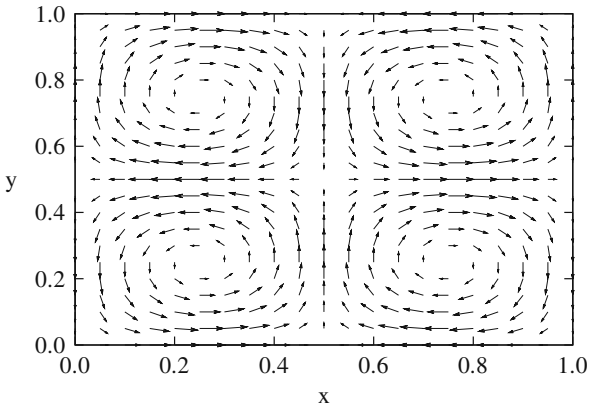

Fig. 2 Snapshot of the velocity field of the convection flow at $t = 0$ computed from the stream function (9)

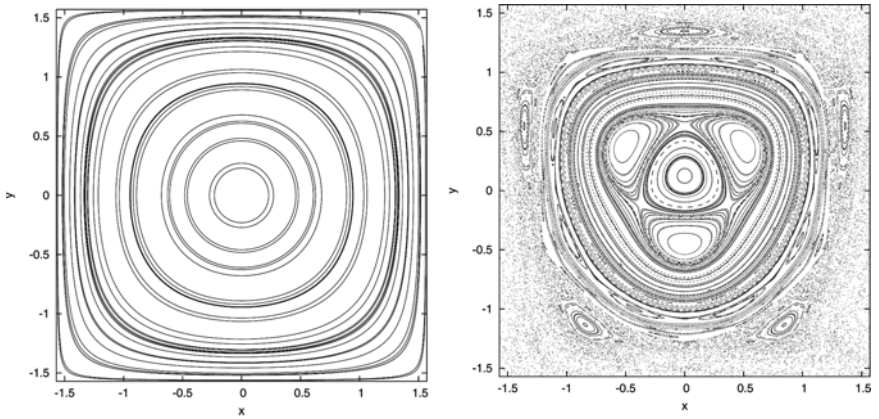

Fig. 3 The cellular flow, Eq.(10). (**a**) The passively advected particles exhibit regular motion if the flow is time-independent ($B = 0$, $k = 1$). The trajectories of 30 particles with randomly selected initial positions are shown. (**b**) Chaotic behaviour in the time-dependent flow ($B = 0.3$, $k = 1$, $\omega = 2.72224$). Snapshots of 200 particles with randomly selected initial conditions are shown at integer multiples of the flow's period

passively advected particles exhibit regular motion; they trace out the closed curves visible in the figure. The rest of the particles fill out the chaotic region. This makes the cellular flow different from the convective flow in that the passive particle motion in the cellular flow, due to the oscillating vortex centres, can be chaotic for $B \neq 0$.

3.3 The Von Kármán Vortex Street

The open flow around an obstacle is a classical problem in fluid mechanics [14, 24]. We consider a viscous incompressible flow around a cylinder of radius R_0. Far away from the obstacle the flow is expected to be uniform. We label the longitudinal flow direction by x, and the transverse direction by y.

Denoting by U the velocity for $x \to \pm\infty$, the Reynolds number associated with this flow can be defined as

$$\mathrm{Re} = 2R_0U/\nu, \tag{11}$$

where ν is the fluid's kinematic viscosity. For Re sufficiently small, the flow is stationary. When Re passes a critical value $\mathrm{Re}_c \approx 80$, the stationary solution of the Navier-Stokes equation becomes unstable, and the flow becomes time-periodic with some period T.

Vortices are created in the wake of the cylinder, detach from it and drift downstream. They gradually weaken owing to the viscosity, until after some distance they vanish. New vortices are shed from the surface of the cylinder at intervals of half a

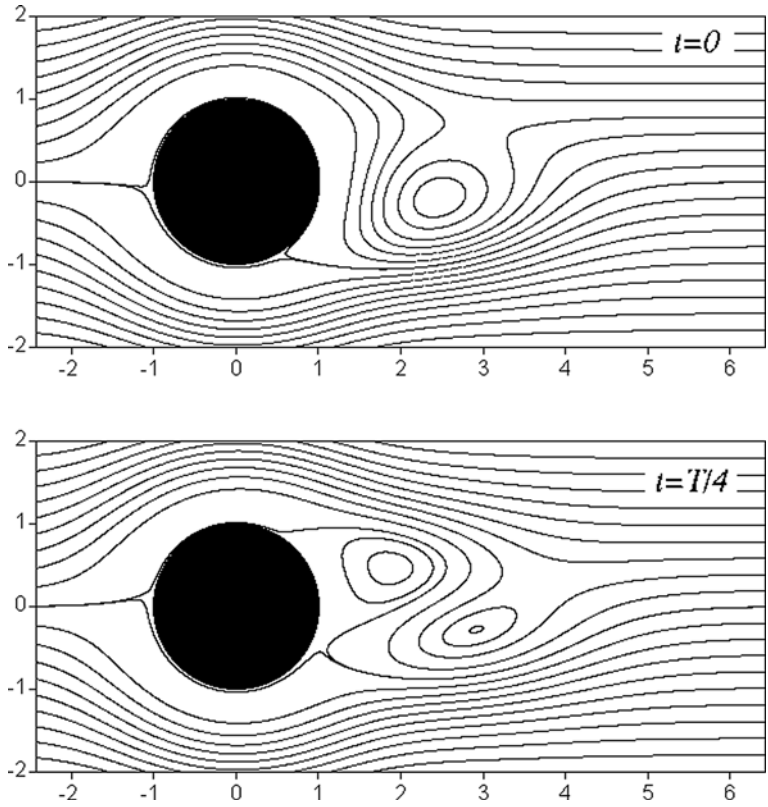

Fig. 4 *Streamlines* for the flow around a cylinder at two different times, separated by one quarter of the full period T of the flow. The vortex shedding is clearly visible

period $T/2$, alternately above and below the middle of the cylinder (see Fig. 4). By this process, a *von Kármán vortex street* is formed behind the cylinder. For simplicity we assume that the lifetime of each detached vortex equals one period T.

An analytical model for the flow in the von Kármán vortex street has been proposed [25, 26], which fits well the results of the direct numerical calculation for $\mathrm{Re} = 250$ [27]. In this model, the stream function $\psi(x,y,t)$ is explicitly given, and we shall use this kinematic model in what follows. This model serves thus as an ideal paradigm for a large class of open chaotic flows and has been widely used to study different aspects of transient chaotic advection (see e.g., [28–30]).

The stream function $\psi(x,y,t)$ can be directly used in Eq. (1) to find the motion of passively advected particles in the von Kármán flow by numerical integration. To appreciate the importance of the unstable manifold of the chaotic saddle, we place a dye droplet of particles upstream into the flow and follow the deformation of the shape of this droplet. Assume that the initial droplet overlaps with the stable manifold of the saddle. Particles that fall exactly on the stable manifold hit the saddle and never leave it. Neighbouring points, however, only approach the saddle; they stay

in its neighbourhood for a while, but sooner or later they leave the wake along the unstable manifold. Thus, we conclude that tracer particles that do not leave a region of observation in the wake too rapidly, must trace out the unstable manifold. In other words, the unstable manifold of the chaotic saddle is a "quasi-attractor" of the tracer dynamics: particles accumulate on it while being advected away. In numerical simulations with a finite number of particles, the manifold serves as a (periodically moving) template, which becomes gradually emptied as more and more particles escape through the outflow.

Figure 5 shows the evolution of a droplet in the von Kármán flow. First the droplet becomes stretched and folded and later it becomes clear that it traces out a moving fractal object, the unstable manifold. Though a few particles are still visible, the region is almost emptied in the last panel; this is a consequence of the finite number of particles used in the simulation.

Note that the von Kármán vortex street is not a particular property of cylindrical obstacles. Most (approximately) two-dimensional flows past an obstacle have this property, provided that their Reynolds number is in the appropriate range. Thus, von Kármán vortices are found in many real situations [31–33].

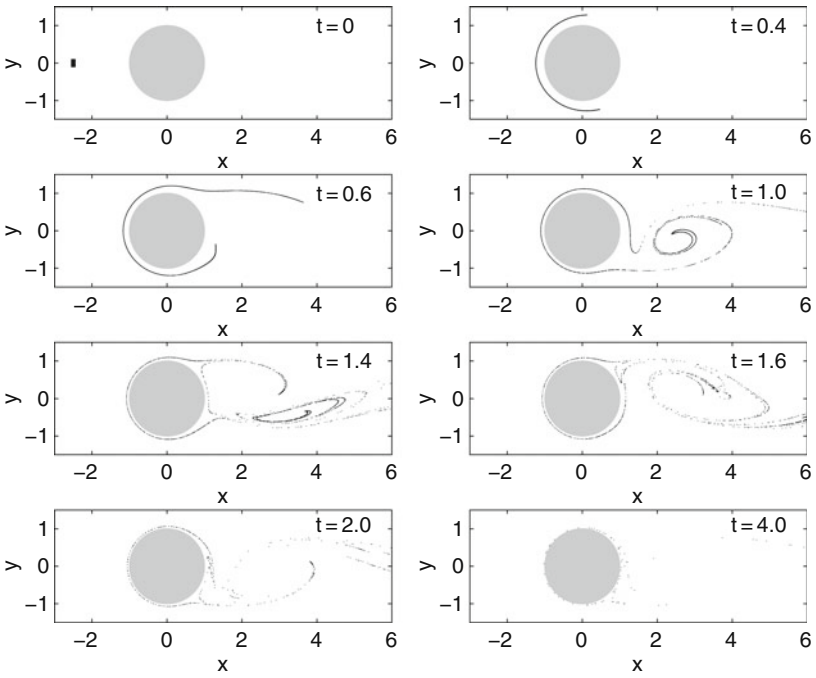

Fig. 5 Time evolution of a droplet of 20,000 tracers in the von Kármán flow shown at different dimensionless times t

4 Inertial Effects in Closed Chaotic Flows

The most general description of the dynamics of finite-size particles presents an enormous richness of phenomena (see, for example, [7, 9, 34–40]). It is characteristic of the dynamics that invariant surfaces in the model without inertia are broken up. For example, as shown for aerosols in Fig. 6, the particles accumulate on higher dimensional attractors instead of being confined by the closed curves shown in Fig. 3b. Figure 6 shows the 2D projection of the attractor located in the four-dimensional phase space of the particle dynamics.

That the invariant curves no longer exist for inertial, finite-size particles is confirmed in Fig. 7. Here, the periodic boundary conditions have been removed from the cellular flow, and the particles are allowed to fly out of the $x,y \in [-\pi/2,\pi/2]$ domain. For passive advection (not shown), the $y = \pm\pi/2$ lines are impenetrable invariant curves; the advected particles can only leave the $x,y \in [-\pi/2,\pi/2]$ domain in the x direction. As shown in Fig. 7 the invariant curves $y = \pm\pi/2$ do not exist for aerosols, which can fly out in the y direction as well.

In the time-independent case, what were invariant surfaces in the model without inertia are transformed into spirals, owing to centrifugal forces: outward spirals for aerosols and inward spirals for bubbles. As a consequence, heavy particles tend to accumulate at the separatrices of the flow.

For large densities $\rho_p \gg \rho_f$, particles are no longer confined within vortices. Stokes drag is the most important force acting in this case, since the added-mass term becomes negligible as $R \to 0$ in this limit (see Eq. (6)) and gravity is not acting on the horizontal plane. So to a first approximation Eq. (5) transforms into

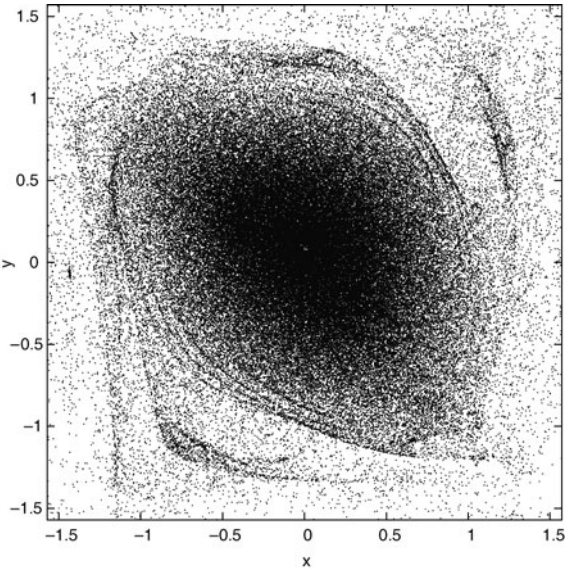

Fig. 6 Aerosols ($R = 0.5$, $\mathrm{St}^{-1} = 0.04$) followed in the cellular flow. The particle positions are shown at integer multiples of the flow's period after 10 periods. The parameters of the flow are the same as those in Fig. 3b

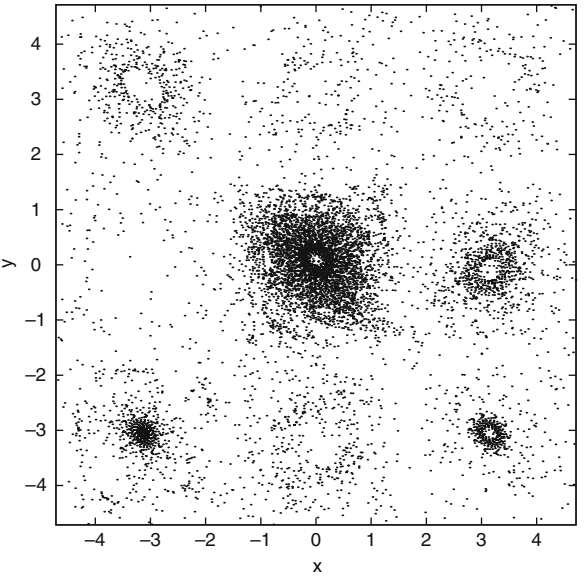

Fig. 7 Aerosols ($R = 0.5$, $\mathrm{St}^{-1} = 0.04$) followed in the cellular flow without periodic boundary conditions. All particles are initiated within the $x,y \in [-\pi/2, \pi/2]$ domain. The particle positions are shown at integer multiples of the flow's period. The parameters of the flow are the same as those in Fig. 3b

$$\frac{d^2x}{dt^2} = -\mathrm{St}^{-1}\left(\frac{dx}{dt} - u_x(x,y,t)\right), \tag{12}$$

$$\frac{d^2y}{dt^2} = -\mathrm{St}^{-1}\left(\frac{dy}{dt} - u_y(x,y,t)\right), \tag{13}$$

and the Stokes number can be written as

$$\mathrm{St}^{-1} = \frac{9\nu\rho_f L}{2a^2\rho_p U}.$$

To derive this we used $m_p = \frac{4}{3}\pi a^3 \rho_p \gg m_f$ in Eq. (6).

This is a highly-dissipative and singular perturbation of a Hamiltonian system, with a four-dimensional phase space:

$$\dot{x} = p_x, \tag{14}$$

$$\dot{p}_x = -\mathrm{St}^{-1}(p_x - u_x(x,y,t)), \tag{15}$$

$$\dot{y} = p_y, \tag{16}$$

$$\dot{p}_y = -\mathrm{St}^{-1}(p_y - u_y(x,y,t)). \tag{17}$$

In the time-dependent case, particles tend to accumulate on a chaotic attractor of the high-dimensional phase space. As the upper panel of Fig. 8 shows for the cellular flow (9), the projection of the attractor on the plane of the fluid lies within the chaotic regions of the model flow without inertia. The relative velocity fluctuates

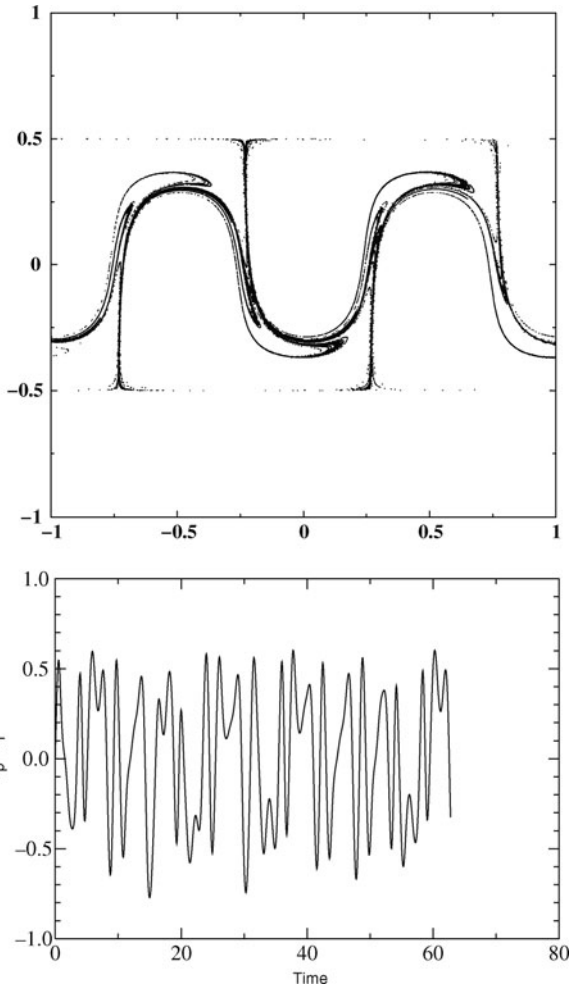

Fig. 8 *Above*: dense particles converge to fractal structures around a separatrix of the flow given by Eq. (10) in the time-independent case. *Below*: in the large inertia limit, the relative velocity of particle and flow fluctuates chaotically, in a Brownian-like fashion

chaotically, due to macroscopic, non-turbulent fluctuations, that act to give the particles deterministic but Brownian-like motion, illustrated in the lower panel of Fig. 8.

4.1 Neutrally Buoyant Particles

Let us now consider whether even in the most favourable case of neutral buoyancy a finite-sized tracer particle remains always close to a flow trajectory [41]. With this in mind, we set $\rho_p = \rho_f$ in Eqs. (5) and (6), which corresponds to setting $W = 0$ and $R = 2/3$:

$$\frac{d\mathbf{v}}{dt} = \frac{D\mathbf{u}}{Dt} - \mathrm{St}^{-1}\,(\mathbf{v} - \mathbf{u})\,. \tag{18}$$

In the past it has been assumed that neutrally buoyant particles have trivial dynamics (e.g., [34, 42]), and the mathematical argument used to back this up is that if we make the approximation $D\mathbf{u}/Dt = d\mathbf{u}/dt$, which can be seen as a rescaling of the added mass, the problem becomes very simple

$$\frac{d}{dt}(\mathbf{v} - \mathbf{u}) = -\mathrm{St}^{-1}(\mathbf{v} - \mathbf{u}). \tag{19}$$

Thence

$$\mathbf{v} - \mathbf{u} = (\mathbf{v}_0 - \mathbf{u}_0) \exp(-\mathrm{St}^{-1}\, t), \tag{20}$$

from which we would infer that even if we release the particle with a different initial velocity $\mathbf{v}_0$ to that of the fluid $\mathbf{u}_0$, after a transient phase the particle velocity will match the fluid velocity, $\mathbf{v} = \mathbf{u}$, meaning that if we accept this argument, a neutrally buoyant particle should be an ideal tracer.

Although from the foregoing it would seem that neutrally buoyant particles represent a trivial limit to Eq. (2), in the argument presented above we did not take the correct approach to the problem, because we did not recognise that $D\mathbf{u}/Dt \neq d\mathbf{u}/dt$. If we substitute Eqs. (3) and (4) for the derivatives into Eq. (18), we obtain

$$\frac{d}{dt}(\mathbf{v} - \mathbf{u}) = -((\mathbf{v} - \mathbf{u}) \cdot \nabla)\,\mathbf{u} - \mathrm{St}^{-1}(\mathbf{v} - \mathbf{u}). \tag{21}$$

We may then write the velocity difference between fluid particle and fluid as $\mathbf{q} = \mathbf{v} - \mathbf{u}$, whence

$$\frac{d\mathbf{q}}{dt} = -\left(-J + \mathrm{St}^{-1} I\right) \cdot \mathbf{q}, \tag{22}$$

where J is the Jacobian matrix:

$$J = \begin{pmatrix} \partial_x u_x & \partial_y u_x \\ \partial_x u_y & \partial_y u_y \end{pmatrix}. \tag{23}$$

If we diagonalise matrix J we obtain the equation for the particle-fluid velocity difference in coordinates aligned with the eigenvectors, which we denote by $\mathbf{q}_D$:

$$\frac{d\mathbf{q}_D}{dt} = \begin{pmatrix} \lambda - \mathrm{St}^{-1} & 0 \\ 0 & -\lambda - \mathrm{St}^{-1} \end{pmatrix} \cdot \mathbf{q}_D. \tag{24}$$

Therefore, if $\mathrm{Re}(\lambda) > \mathrm{St}^{-1}$, $\mathbf{q}_D$ may grow exponentially. Now λ satisfies $\det(J - \lambda I) = 0$, so $\lambda^2 - \mathrm{tr}J + \det J = 0$. Since the flow is incompressible, $\partial_x u_x + \partial_y u_y = \mathrm{tr}J = 0$, thence $-\lambda^2 = \det J$. Given squared vorticity $\omega^2 = (\partial_x u_y - \partial_y u_x)^2$, and squared strain $s^2 = s_1^2 + s_2^2$, where the normal component is $s_1 = \partial_x u_x - \partial_y u_y$ and the shear component is $s_2 = \partial_y u_x + \partial_x u_y$, we may write

$$\lambda^2 = -\det J = (s^2 - \omega^2)/4 = Q. \tag{25}$$

Here $Q = (s^2 - \omega^2)/4$ is the so-called Okubo–Weiss parameter [43, 44]. If $Q > 0$, $\lambda^2 > 0$, and λ is real, deformation dominates, as around hyperbolic points. If $Q < 0$, $\lambda^2 < 0$, and λ is complex, rotation dominates, as near elliptic points. Equation (22) together with $d\mathbf{r}/dt = \mathbf{q} + \mathbf{u}$ defines a dissipative dynamical system

$$d\boldsymbol{\xi}/dt = \mathbf{F}(\boldsymbol{\xi}) \tag{26}$$

with $\boldsymbol{\xi} = (\mathbf{r},\mathbf{q})$. Equation (26) has constant divergence $\nabla \cdot \mathbf{F} = -2/\mathrm{St}$ in the four dimensional phase space of $\boldsymbol{\xi}$. While small values of St allow for large values of the divergence, large values of St force the divergence to be small. The Stokes number is the dimensionless decay time of the particle (see Sect. 2.1): with larger St, the particle has more independence from the fluid flow. From Eq. (24), in areas of the flow near hyperbolic stagnation points with $Q > \mathrm{St}^{-2}$, particle and flow trajectories separate exponentially.

To illustrate the effects of St and Q on the dynamics of a neutrally buoyant particle, let us consider the simple incompressible two-dimensional model (10). In Fig. 9 (top left) the contours of Q are depicted. Notice that the high values of Q are around the hyperbolic points, while negative Q coincides with the centres of vortices – elliptic points – in the flow. Figure 9 (top right) shows the trajectory of a neutrally buoyant particle starting from a point on a fluid trajectory within the central vortex, but with a small velocity mismatch with the flow. This mismatch is amplified in the vicinity of the hyperbolic stagnation points where Q is larger than St^{-2} to the extent that the particle leaves the central vortex for one of its neighbours. In the end a particle settles on a trajectory that does not visit regions of high Q, as expected for a fluid parcel. While this effect is already seen in Fig. 9 (top right), it is more dramatically pictured in the trajectory shown in Fig. 9 (bottom left), in which the particle performs a long and complicated excursion wandering between different vortices before it settles in a region of low Q. To illustrate the divergence of particle and fluid trajectories, and the fact that particle and fluid finally arrive at an agreement, in Fig. 9 (bottom right) we display the difference between the particle velocity and the fluid velocity at the site of the particle against time for this case. Notice that this difference seems negligible at time zero, and that it also convergences to zero at long times, but during the interval in which the excursion takes place it fluctuates wildly.

Even more interesting is the case of time-dependent flows: $B \neq 0$ in our model. As in a typical Hamiltonian system, associated with the original hyperbolic stagnation points, there are regions dominated by chaotic trajectories. Trajectories of this kind, stroboscopically sampled at the frequency of the flow, are reproduced in Fig. 10. Such trajectories visit a large region of the space, which includes the original hyperbolic stagnation points and their vicinities where Q is large. Excluded from the reach of such a chaotic trajectory remain areas where the dynamics is regular: KAM tori. In our model these lie in the regions where $Q < \mathrm{St}^{-2}$. A neutrally buoyant particle trying to follow a chaotic flow pathline would eventually reach the highly

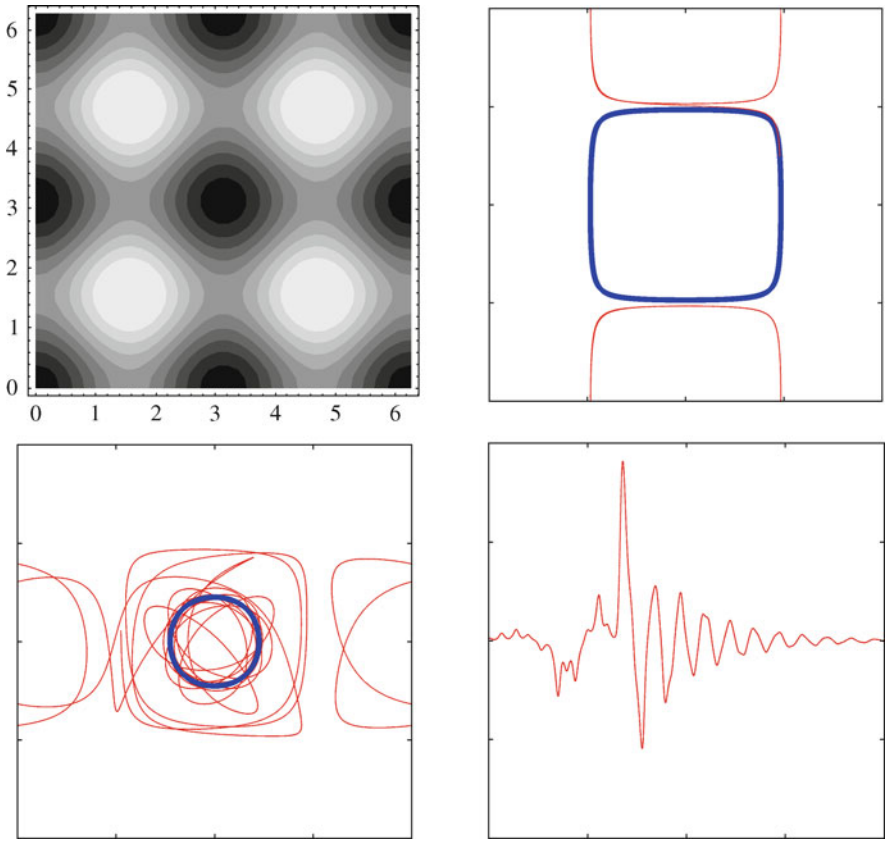

Fig. 9 (*Top left*) Contour plot illustrating magnitude of Q – lighter is higher Q – for the time-independent model Eq. (10) (the flow is on a torus). (*Top right*) The separation of a neutrally buoyant particle trajectory (*thin line*) from the flow (*thick line*) in regions of high Q allows the particle to wander between cells. (*Bottom left*) After a complicated excursion, a particle (*thin line*) eventually settles in a zone of low Q of the flow; a KAM torus (*thick line*). (*Bottom right*) The velocity difference $v_x - u_x$ between the particle and the flow against time

hyperbolic regions of the flow. This makes likely its separation and departure from such a pathline, in search of another pathline to which to converge. However, convergence will only be achieved if the pathline never crosses areas of high Q. Figure 10 demonstrates this phenomenon: a particle was released in the chaotic zone with a small velocity mismatch. The particle followed the flow, until, coming upon a region of sufficiently high Q, it was thrown out of that flow pathline onto a long excursion that finally ended up in a regular region of the flow on a KAM torus. The regular regions of the flow then constitute attractors of the dissipative dynamical system Eq. (26) that describes the behaviour of a neutrally buoyant particle. The chaotic trajectories in a Hamiltonian system are characterised by positive Lyapunov exponents. The Lyapunov exponents are an average along the trajectory of the local rate

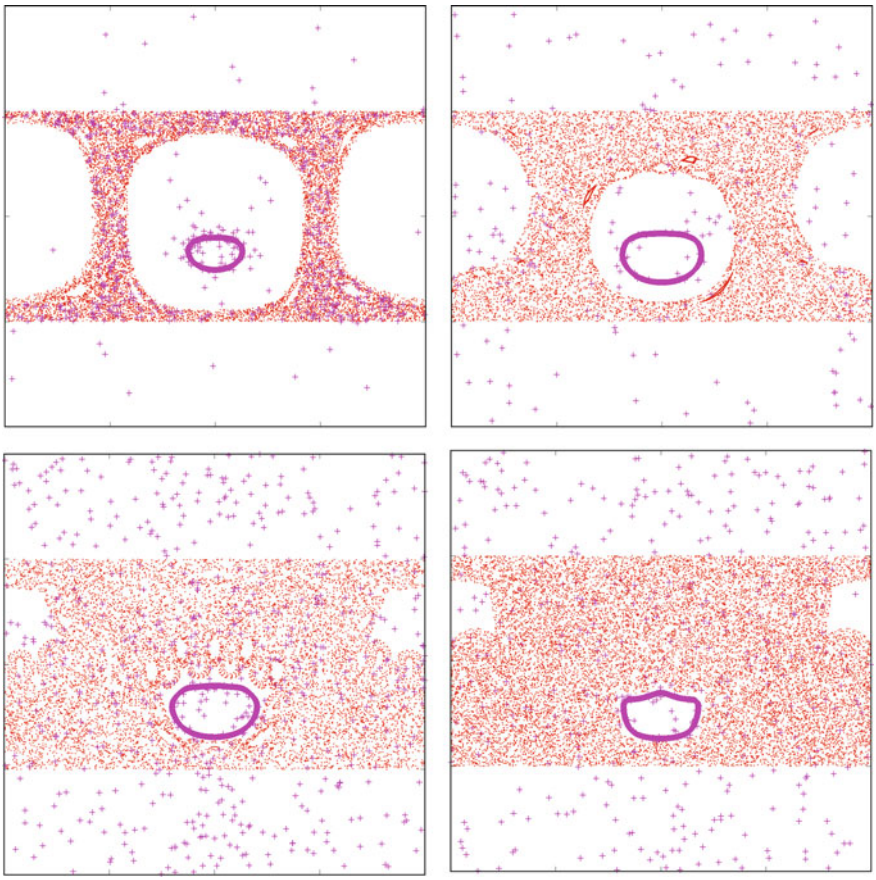

Fig. 10 Poincaré sections of trajectories in the time-dependent flow of Eq. (10). From *top left* to *bottom right* are shown (*dots*) four increasingly chaotic examples of the flow, and (crosses), the trajectories of neutrally buoyant particles in the flows that in each case finally end up on a KAM torus within the regular region of the flow

of convergence or divergence. Hence, for a trajectory to be chaotic, it is a necessary condition that it visit regions of positive Q: an upper bound to Q is an upper bound to the Lyapunov exponent.

Consider the implications of these results for two-dimensional turbulent flows, in which Q defines three regions: in the vortex centres it is strongly negative; in the circulation cells that surround them, strongly positive, while in the background between vortices it fluctuates close to zero (see, e.g., [45–49]). As a result of the dynamics, an initially uniform distribution of neutrally buoyant particles with finite size evolves in time towards an asymptotic distribution concentrated in the inner part of vortices where $Q < 0$, and with voids in the areas crossed by fluid trajectories that visit regions where $Q > \mathrm{St}^{-2}$, as we illustrate in Fig. 11.

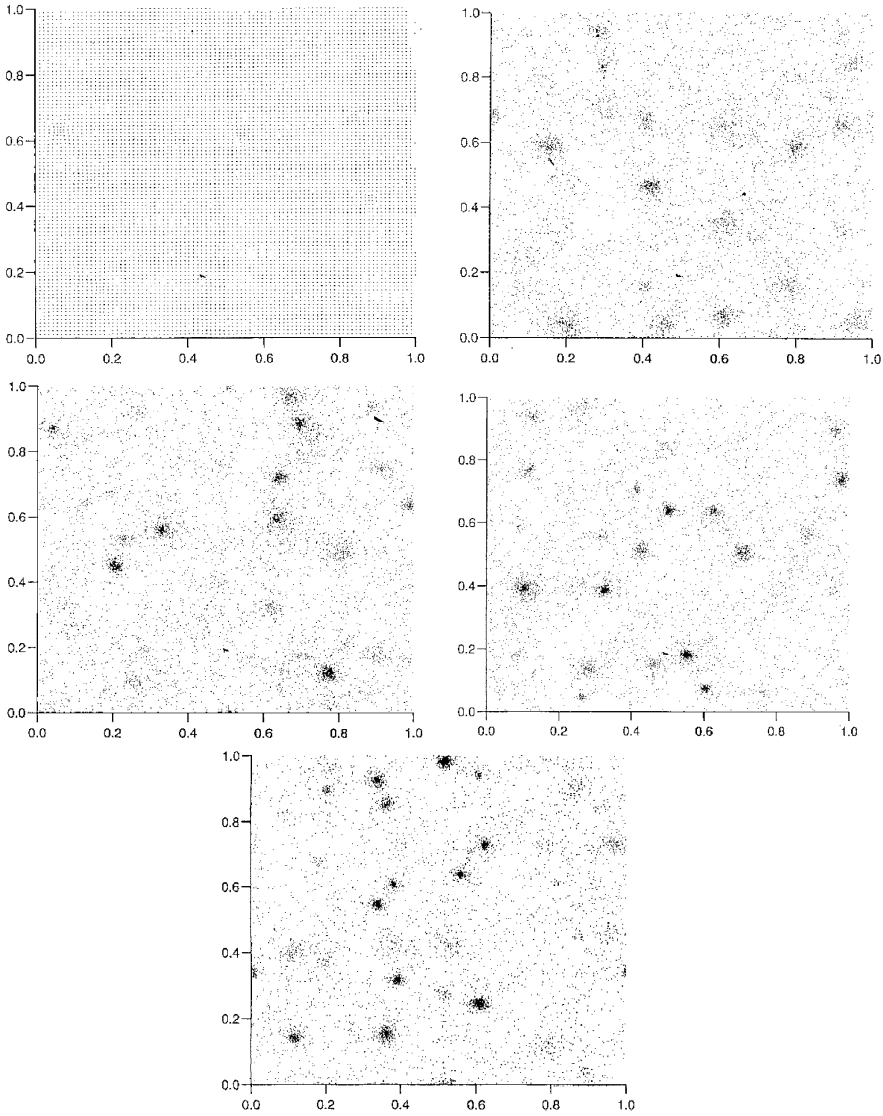

Fig. 11 Small neutrally buoyant tracer particles converge to the centres of vortices in a two-dimensional turbulent flow simulation; distribution at times (*top left* to *bottom right*) $t = 1$, 2, 3, 4, and 6 of particles uniformly distributed in the flow at time $t = 1$ [41]

Thus even with a small rigid neutrally buoyant spherical tracer particle in an incompressible two-dimensional fluid flow the tracer trajectories can separate from the fluid trajectories in those regions where the flow has hyperbolic stagnation points. For flows with chaotic pathlines, analysis shows that the tracer will only evolve on trajectories having Lyapunov exponents bounded by the value

of the Stokes drag coefficient. Therefore, by making the value of this coefficient small enough, one can force the tracer to settle on either the regular KAM-tori dominated regions or to selectively visit the chaotic regions with small Lyapunov exponents. As well as its interest from the viewpoint of dynamical systems, this result is important to the analysis of observations and experiments with neutrally buoyant particles both in the laboratory and in the atmosphere and oceans.

The heuristic criterion for the departure of trajectories of neutrally buoyant particles trajectories from those of the fluid elements has been complemented by more rigorous analysis. For example, the stability of the fluid flow manifold which is invariant under the neutrally buoyant particle dynamics was studied in the more general context of the perturbed invariant manifold of the non-neutral particles [50, 51]. For neutrally buoyant particles, this analysis parallels a previous interpretation of the fluid invariant manifold as a "bailout embedding" and the departure of trajectories as a "blowout bifurcation" taking place as the Stokes number is varied [52]. In both cases, it has been found that the heuristic criterion based on the Okubo-Weiss parameter underestimates the areas of departure. Finally noise or fluctuating forces enhance the phenomenon, as has been rigorously proved in [53].

4.2 3D Flows and Bailout Embeddings

For incompressible two-dimensional flows, since the Jacobian matrix is traceless, the two eigenvalues must add up to zero, which implies that they are either both purely imaginary or both purely real, equal in absolute value and opposite in sign. The result is that the particles can abandon the fluid trajectories in the neighbourhood of the saddle points and other unstable orbits, where the Jacobian eigenvalues are real, and eventually overcome the Stokes drag, to finally end up in a regular region of the flow on a KAM torus dominated by the imaginary eigenvalues. From a more physical point of view, this effect implies that the particles tend to stay away from the regions of strongest strain.

In contrast to the two-dimensional case, in time-dependent 3D flows the incompressibility condition only implies that the sum of the three independent eigenvalues must be zero. This less restrictive condition allows for many more combinations. Triplets of real eigenvalues, two positive and one negative or vice versa, as well as one real eigenvalue of either sign together with a complex-conjugate pair whose real part is of the opposite sign, are possible. Accordingly, chaotic trajectories may have one or two positive Lyapunov numbers, and a richer range of dynamical situations may be expected.

Note that the dynamical system governing the behaviour of neutrally buoyant particles is composed of a lower-dimensional dynamics within a "larger", higher-dimensional dynamics. Equation (18) can be seen as an equation for the variable $\mathbf{q} = (\mathbf{v} - \mathbf{u})$ which in turn defines the equation of motion ($\dot{\mathbf{r}} = \mathbf{u}$) of a fluid

element whenever the solution of the former is zero. In this sense we may say that the fluid parcel dynamics is embedded in the particle dynamics. In reference to the fact that some of the embedding trajectories abandon some of those of the embedded dynamics, the generalisation of this process is dubbed a *bailout embedding* [52].

Consider neutrally buoyant particles immersed in a flow in which each component of the velocity vector field is sinusoidally modulated with a relative phase shift of $2\pi/3$ and where x, y, and z are to be considered $(\mathrm{mod}2\pi)$

$$\begin{aligned}
\frac{dx}{dt} &= (1 + \sin\ 2\pi t) \cdot (A \sin z + C \cos y), \\
\frac{dy}{dt} &= \left(1 + \sin\ 2\pi \left(t + \frac{1}{3}\right)\right) \cdot (B \sin x + A \cos z), \\
\frac{dz}{dt} &= \left(1 + \sin\ 2\pi \left(t + \frac{2}{3}\right)\right) \cdot (C \sin y + B \cos x).
\end{aligned} \tag{27}$$

This is a modified version of the ABC flow [54]. This flow shows structures consisting of a complex array of KAM sheets and tubes surrounded by chaotic volumes [55]. Neutrally buoyant particles show a tendency to accumulate inside KAM tubes as depicted in Fig. 12, where ten particles, initially distributed at random in the cubic cell, are shown to end up in the interior of two of the tubes.

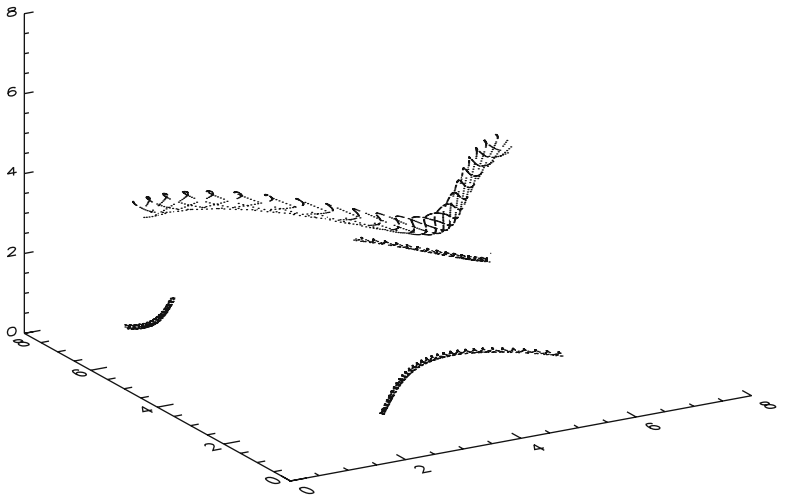

Fig. 12 Stroboscopic sampling (with period T=1) of the position of 10 particles initially distributed at random in a flow described by Eq. (27) with $A = 2$, $B = 0.4$, $C = 1.2$. The *dots* represent the positions of these particles at the strobing periods 1,000–2,000

5 Advection of Finite-Size Particles in Open Flows

Here we concentrate on the question of how the global dynamics of advection changes in two-dimensional open flows due to inertia. As discussed in Sect. 2, one big difference between finite-size and non-inertial particles is that the dynamics of the former is dissipative, which opens the possibility of the existence of attractors. In the flow model of the von Kármán vortex street of Sect. 3.3, it has been found that attractors are possible in the bubble regime $2/3 < R < 2$. Light particles might thus *become trapped* in the wake forever. For $R = 1.33$, $\mathrm{St}^{-1} = 30$ there are, for instance, three coexisting attractors [56–58]: two fixed points around the cylinder's surface and one at $x = \infty$.

To gain insight into what happens to ensembles of bubbles, the residence time in a region around the cylinder is determined. The initial velocities were set to be equal to the flow velocity. Figure 13 shows the result, where grey, white and black depict increasingly long residence times. Dark regions mark permanently trapped particles. This region corresponds thus to the basin of attraction of the two finite attractors, which is in fact a projection of the basin structure in the full phase space on the plane of the flow. At other inertia parameters there also exist chaotic saddles which ensure that the approach toward the attractors, including the escape from the wake (the approach toward the attractor at $x = \infty$) is a transient chaotic process.

A systematic investigation of the escape rate $\kappa(\mathrm{St})$ from the hyperbolic parts of this saddle shows (Fig. 14) that the escape rate is *below* the escape rate of fluid parcels or passive tracers in the full range $\mathrm{St}^{-1} > 12$. This indicates that bubbles spend much more time in the wake than fluid particles. In the interval $14 < \mathrm{St}^{-1} < 45$ the escape rate vanishes indicating the presence of attractors. For St^{-1} in between 33 and 45 these attractors are chaotic. Beyond 45 the escape rate is positive, and it approaches for large St^{-1} the value of ideal tracers.

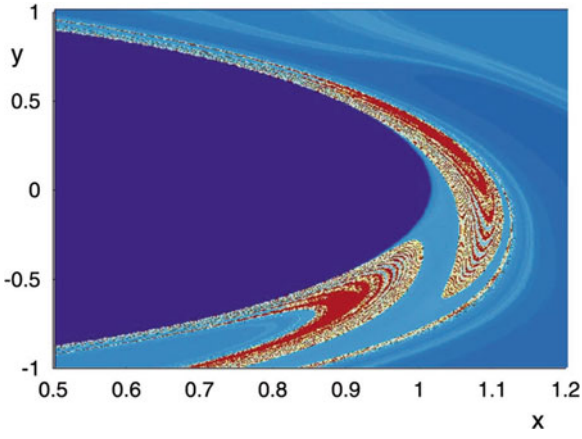

Fig. 13 Finite-size particles in the von Kármán flow. Residence time for bubbles of parameter $\mathrm{St}^{-1} = 30$, $R = 1.33$ ($g = 0$) at $t = 0.3$ mod 1. Basins of attraction of two chaotic attractors appear *shaded dark* in the plane of the fluid. From [57]

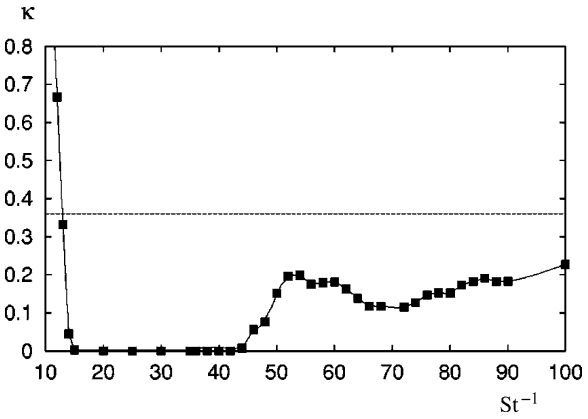

Fig. 14 Escape rate as a function of the Stokes number in the bubble regime ($R = 1.7$). The *horizontal line* is the escape rate for passive tracers. From [57]

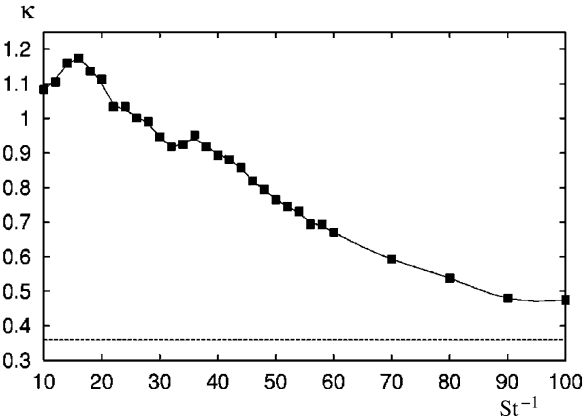

Fig. 15 Escape rate as a function of the Stokes number in the aerosol regime ($R = 0.5$). The *horizontal line* is the escape rate for passive tracers. From [57]

The tendency is opposite for aerosol particles. The escape rate is *above* the escape rate of fluid particles for any value of St, i.e. heavy particles spend much less time in the wake than fluid particles (Fig. 15).

There is a qualitative argument explaining why bubbles tend to form attractors. The particles are typically subject to local vortices. The centrifugal force for a particle comoving with a vortex is proportional to the density difference $\rho_p - \rho_f$. For heavy particles this force pushes particles outward, but for light ones it attracts particles toward the vortex centre. The presence of this centripetal force is an important reason for the existence of bubble attractors. The mechanism is similar to an observation of Maxey [12] according to which aerosols (bubbles) settle in the presence of gravity faster (slower) in turbulent flows than in a fluid at rest. The explanation of this phenomenon is the centrifugal (centripetal) effect of the turbulent vortices.

As a consequence of the dependence of the dynamics on particle parameters, when starting from a mixture of particles of the same density but of different size, segregation can be observed in chaotic flows consisting of a sequence of obstacles. As an example of this type of flow, we consider an infinite chain of cylinders situated

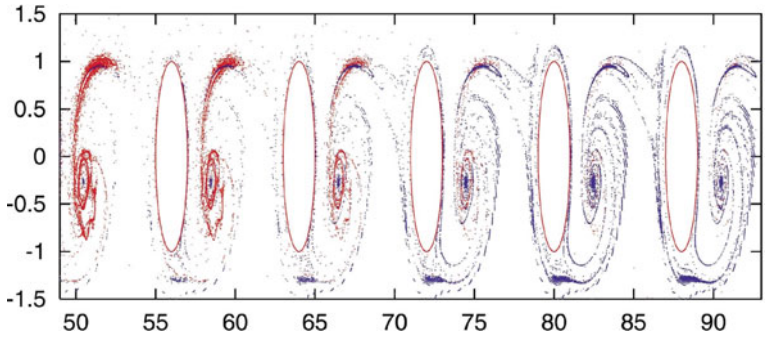

Fig. 16 Separation of bubbles in a chain of cylinders. The distribution of particles with $R = 1.4$ and $\mathrm{St}^{-1} = 20$ $\mathrm{St}^{-1} = 120$ coloured *red* and *blue*, respectively, after 10 time units. The initial location is a *small square* with uniformly mixed particles in front of the cylinder located at the origin. From [57]

at a distance of 8 cylinder radii from each other. The initial droplet of particles contains a uniform mixture of particles of $\mathrm{St}^{-1} = 20$ (red) and $\mathrm{St}^{-1} = 120$ (blue), and is injected into the flow in front of the cylinder centred at the origin. After passing several cylinders, the droplet exhibits a clear separation as shown in Fig. 16. The larger light particles ($\mathrm{St}^{-1} = 20$) escape more slowly due to the centripetal effect of the vortices. The flow in the cylinder chain acts therefore as a chaotic chromatograph [57].

A work worthy of note is that of Haller and coworkers [50, 59]. They show that for small particle sizes, i.e., for small Stokes numbers ($\mathrm{St} \ll 1$), the dynamics of a finite-size particle can be approximated by the dynamics on a low-dimensional inertial manifold, which can be calculated explicitly from a given velocity field. Following an approach of Maxey [12], they show that after a short transient time the equation of motion of such small inertial particles can well be approximated by the equation, termed inertial equation in [50]

$$\dot{\mathbf{r}}(t) = \mathbf{u}(\mathbf{r}(t),t) + W\mathbf{n} + \mathrm{St}\left(\frac{3}{2}R - 1\right)\frac{D}{Dt}\mathbf{u}(\mathbf{r}(t),t). \tag{28}$$

This can formally be obtained by expanding Eq.(5) around its $\mathrm{St} = 0$ solution: $\dot{\mathbf{r}}(t) = \mathbf{u} + W\mathbf{n}$ up to first order in St. The advantage of this equation becomes clear when tracing particles backwards in time.

Finding a localised source of particle release is often of central relevance. Such a source-inversion problem appears, for example, in locating a source of air-transported contaminant particles. The approach based on the time-reversed integration of Eq. (5) leads to an unavoidable numerical instability due to an exponential growth of the type $\exp(t/\mathrm{St})$. In contrast, the inertial equation (28) is free from this instability. It can be solved easily in reverse time, too, and this procedure provides with good accuracy the initial spatial coordinates of inertial particles. This has been clearly demonstrated in the example of bubbles in the von Kármán flow [50], and

in other realistic cases like e.g., anthrax in the wind field of an urban street canyon [60] and aerosols in the flow of a hurricane [61].

In spite of the repelling centrifugal force for heavy particles, Vilela and Motter showed [62] that aerosols can also be trapped by open flows under certain circumstances. Such aerosol attractors can exist due to a special interplay of two or more vortices.

In the case of neutrally buoyant particles, $R = 2/3$, in an open chaotic flow, the effect of inertia is to cause a dispersion of particles around the fractal structure of the unstable chaotic set which exists for perfect tracers [63]. Since the introduction of inertia enlarges the phase space to a 4-dimensional manifold (for 2D flows), it is no surprise that the properties of the motion on the 2-dimensional projection to the configuration space are different from its non-inertial counterpart. The important point is that, for small Stokes numbers, the distribution of long-lived inertial particles can still be understood in terms of the simple chaotic set of the non-inertial dynamics. In [63], an expression is derived for the dispersion of particles around the inertia-less chaotic set, which agrees well with numerical simulations. The main result of this work is that inertia causes the fractal structure of the chaotic set to be lost in the configuration space, so that below a certain scale determined by the Stokes number, the spatial distribution becomes smooth. In the slow manifold approach of Haller and coworkers, the slow dynamics coincides with that of infinitesimally small ideal tracers; for $W = 0$, they find that $\dot{\mathbf{r}}(t) = \mathbf{u}$, as can also be seen from (28). Therefore the particle dynamics should synchronise with Lagrangian tracer motion. It has been shown [51], however, that the slow manifold has domains that repel nearby trajectories, which explains the numerical findings of [63].

6 Coagulation and Fragmentation of Finite-Size Particles

So far we have only discussed the motion of passive finite-size particles which are carried by the flow but do not interact with each other. But there is an increasing interest in the investigation of the dynamics of active finite-size particles. The active processes taken into account can be of different natures depending on the context.

In ecology these active finite-size particles, usually aerosols heavier than the fluid, can be plankton species in a limnic or marine environment where plankton populations change their number due to growth and death. Additionally competition and predator-prey interactions influence their dynamics. Particles of different sizes gather along different attractors, as explained in the previous Sections, and therefore different species are expected to occupy different niches, which promotes the coexistence of competitors.

In chemical reactions the active finite-size particles are often bubbles (lighter than the fluid) containing catalysts which mediate particular chemical reactions.

The example which is discussed here in more detail concerns the process of coagulation and fragmentation of finite-size particles in the presence of gravity, which plays an important role in cloud physics [64], marine snow and sediment dynamics

[65, 66], engineering [67], planet formation [68] as well as wastewater treatment [69]. In all the cases mentioned above particles are assumed to interact very rarely, i.e., a kind of "dilute gas" assumption is used.

Coagulation and fragmentation are two processes which influence the size of the particles. Coagulation can happen when two particles collide and form a larger coagulate due to some adhesive forces [64]. Fragmentation is the break-up of a large aggregate into a few smaller ones due to shear forces in the fluid. The dynamics of a system including coagulation and fragmentation is more complicated than the pure advection of finite-size particles. The difficulty lies in the different sizes of the coagulates being advected by the fluid. Because of the dilute approximation, we can assume that the motion of all particles follows the Maxey-Riley equation (5). Coagulates of different sizes correspond to different parameters, namely different Stokes number St and settling velocity W in these equations. Instead of one dynamical system one has to deal with a set of dynamical systems, each of them corresponding to a certain coagulate size. Moreover, the number of coagulates in each dynamical system is changing continuously due to coagulation and fragmentation.

Coagulates of different size converge to different attractors [70] which can be either fixed points, periodic motions, quasiperiodic motions on tori or chaotic attractors (cf. Fig. 17). Among the latter we find a variety of different forms from very localised ones up to space filling attractors where coagulates are distributed over the whole configuration space. As a consequence coagulates of different size are located in different parts of the configuration space in the long-term limit. Hence, a system containing coagulates of different sizes is characterised by an overlay of different attractors possessing possibly different dynamical properties. However, since coagulation and fragmentation happen usually on much smaller time scales than convergence to the attractor, the overall dynamics is in general transient and only a blurred structure of the attractors will be observable.

The same arguments apply to systems where the finite-size particles are bubbles instead of aerosols. Bubbles and aerosols of the same size will occupy different regions in configuration space and exhibit a different kind of dynamics. Therefore, the dynamics of bubbles and aerosols as well as their changes (bifurcations) with

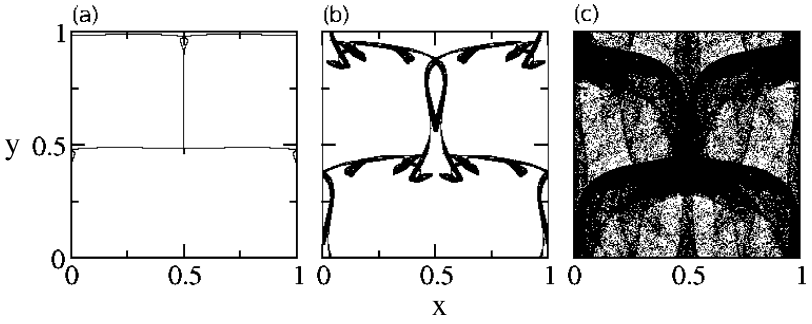

Fig. 17 Attractors for 3 different size classes in a convection flow (9) (cf. Sect. 3.2 for the flow parameters). (**a**) $\mathrm{St}^{-1} = 7.0$, (**b**) $\mathrm{St}^{-1} = 2.778$, (**c**) $\mathrm{St}^{-1} = 2.253$ and $W = 0.4/A$ in all cases

respect to variations of their size are completely different even in the case where their sizes are identical [70]. Finally it is important to note that the form of the attractors depends crucially on the flow [71, 62, 72].

Let us assume that there is a smallest particle in the system which cannot be fragmented. We call it primary particle with radius a_1, mass m_1, Stokes number St_1 and settling velocity W_1. To distinguish the different sizes of the coagulates it is convenient to introduce a size class index α corresponding to the number of primary particles that make up the coagulate. The radius of the coagulate is then $a_\alpha = \alpha^{1/3} a_1$, its Stokes number can be expressed as $\mathrm{St}_\alpha = \alpha^{2/3}\mathrm{St}_1$, and its settling velocity is $W_\alpha = \alpha^{2/3} W_1$; here we see that W/St is independent of α, as discussed at the end of Sect. 2.1. To derive these relations we assume that the coagulates are spherical particles with radius a_α. This assumption applies well to raindrops, while it is a crude approximation for marine aggregates. Marine aggregates are composites of an inorganic kernel like silt or clay with organisms like algae and bacteria attached to it which make up a fractal structure for the whole aggregate. Hence the shape of marine aggregates is more a fractal object than a spherical one.

Coagulation results from a collision of two particles of radii a_i and a_j forming a coagulate of radius $a_{\mathrm{new}}^3 = a_i^3 + a_j^3$ owing to mass conservation. This implies that the size class index of the new coagulate follows from $\alpha_{\mathrm{new}} = \alpha_i + \alpha_j$ which enters $\mathrm{St}_{\mathrm{new}}$ and W_{new}. The velocity of the newly formed coagulate is determined by momentum conservation.

The mechanisms of fragmentation are more complex. While raindrops break apart when they reach a certain maximum size, marine aggregates split up owing to shear forces in the fluid. In the latter case there exists a critical shear force which has to be larger than the intrinsic binding forces of the coagulate to lead to fragmentation. The strength of these binding forces can be measured in terms of a parameter called coagulate strength. For large enough shear forces which overcome the critical shear force a coagulate splits into two smaller ones (determined by a splitting rule, see below). Their velocities are equal owing to momentum conservation and their location is assumed to be directly neighbouring to each other in a random orientation. If the binding force of one of the new smaller coagulates is again smaller than the critical shear force, then an additional break-up takes place. This way more than two new coagulates can result from a single fragmentation event.

Implementing coagulation and fragmentation in the way described above the dynamics of the system can be simulated for different fluid flows. For all subsequent figures concerning coagulation and fragmentation the convection flow explained in Sect. 3.2 is used. Similar results can be obtained for the sine shear flow [72]. In any case one obtains a steady size distribution of coagulates where coagulation and fragmentation balance each other. The shape of the asymptotic size distribution depends on several factors.

Firstly, the size distribution depends on the fluid flow. Secondly, the shape of the size distribution is crucially dependent on the mechanism of fragmentation. While the realization of coagulation is rather straightforward and does not influence the shape of the size distribution, fragmentation needs a more detailed knowledge about the break-up processes to be taken into account. Two different properties of the

fragmentation process are important to consider: (i) what is the critical shear force (splitting condition), how it depends on the size of the coagulate and on the intrinsic binding strength or coagulate strength and, (ii) what is the size distribution of the two fragments created (splitting rule).

To quantify differences in the size distributions depending on various parameters characterising either the flow or the active processes it is convenient to define the average size class index $\langle \alpha(t) \rangle = \sum_\alpha \alpha N_\alpha(t)/N(t)$, where $N_\alpha(t)$ denotes the number of coagulates in size class α, while $N(t)$ is the total number of coagulates in the system. Note that the total number of coagulates always changes in time owing to coagulation and fragmentation. As time evolves $\langle \alpha(t) \rangle$ is found to always reach a limiting value α_∞ though still fluctuating. This implies that a steady size distribution sets in, which is unique, i. e., one finds the same distribution for almost all initial conditions.

Let us now discuss the dependence of the size distribution on the details of the fragmentation process. Unfortunately there are only a few experimental studies devoted to the fragmentation process [73, 74]. Due to this limited knowledge about the details of fragmentation an inverse modelling process has to be considered of making several assumptions about fragmentation and asking which of those yield size distributions which are qualitatively in agreement with observations. In this way one is able to find indications for the most probable fragmentation mechanism.

Fragmentation is modelled by two different mechanisms which occur simultaneously: On the one hand shear forces in the fluid lead to *shear fragmentation* as is typical for marine aggregates and, on the other hand, *size limiting fragmentation* splits all coagulates of a predefined maximum size as is typical for rain drops. The latter break-up process is assumed to be present in shear fragmentation as well. It is known that larger coagulates are more fragile and, hence, fragment more easily. In shear fragmentation the following ansatz for the critical velocity difference Δu_c across a coagulate of size a_α is made:

$$\frac{\Delta u_c}{a_\alpha} \sim \gamma \alpha^{-1/3} \tag{29}$$

where γ is the coagulate strength: a change of this parameter corresponds to considering different types of coagulates. This ansatz is also supported by Taylor [75] and Delichatsios [76] who derived an expression for the critical velocity gradient for the break-up of spherical liquid drops depending on surface tension and viscosity of the drop.

Using Eq. (29) the average size class index is essentially determined by the coagulate strength γ measuring the intrinsic binding strength of the coagulate. With increasing γ the limiting average size class index α_∞ has been found to grow in simulations [72, 77] as

$$\alpha_\infty \sim \gamma^{1/3} \tag{30}$$

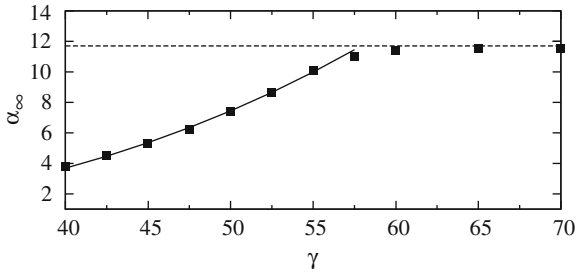

Fig. 18 Asymptotic average size class index α_∞ vs. coagulate strength γ for $\mathrm{St}_1^{-1} = 55.0$, $W_1 = 3.2\mathrm{St}_1$, $\alpha_{\max} = 30$, $a_{\max} = 5 \times 10^{-5}$

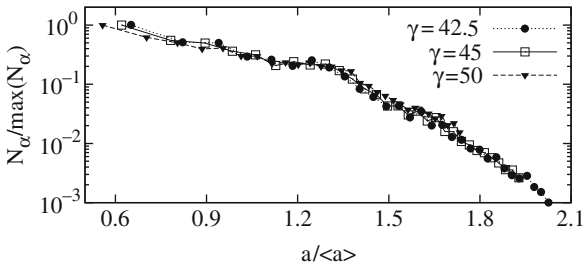

Fig. 19 Normalised size distributions for different coagulate strengths vs. a_α/α_∞ for $\mathrm{St}_1^{-1} = 7.0$, $W_1 = 0.4\mathrm{St}_1$. We started with an initial condition of 10^6 particles with radius $a_1 = 1.5 \times 10^{-5}$

until it reaches (at larger values of γ) a constant finite value (Fig. 18). In the latter interval of γ fragmentation is exclusively dominated by size limiting fragmentation since the binding forces are too strong to allow for shear fragmentation.

In a certain intermediate range of γ where shear fragmentation dominates, all size distributions collapse onto a master curve as shown in Fig. 19 if the steady state size distribution is represented in a normalised form according to $N_\alpha / \max(N_\alpha)$ vs. a_α/α_∞.

As already mentioned the splitting rule determining the size of the two fragments after breaking apart is another important detail of the fragmentation process which can possess several forms. Three different splitting rules have been taken into account in numerical experiments to investigate their impact on the steady size distribution of coagulates: *Uniform splitting* describes a break-up where the size of the first fragment is chosen randomly from a uniform distribution between the smallest size class index 1 and the size class index of the coagulate before splitting α_{old}. For *large scale splitting* the two fragments are of almost equal size, which is expressed mathematically by $\alpha_1 = \alpha_{\mathrm{old}}/2 - |\xi|$ where ξ is a random number (rounded towards the nearest integer) from a normal distribution with zero mean and standard deviation 1, that is cut off at $\pm(\alpha_{\mathrm{old}} - 1)$. *Erosion* corresponds to a break-up where the size of the first fragment is much smaller than the other one, so that $\alpha_1 = |\xi|$ with ξ defined as for large scale splitting.

Numerical simulations show that the shape of the steady size distribution depends crucially on the applied splitting rule. While for erosion and uniform splitting the smallest size class contains most of the coagulates, large scale splitting yields a size distribution with a pronounced maximum at rather small size classes and an exponential decay towards larger size classes (Fig. 20). Particularly this exponential tail

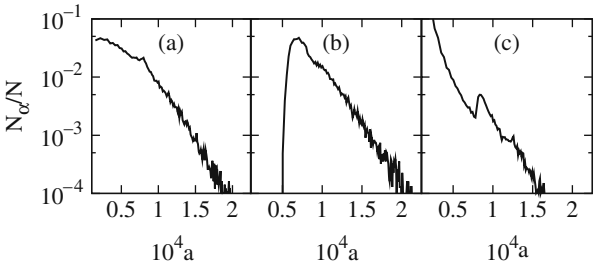

Fig. 20 Size distributions for different splitting rules (**a**) uniform splitting, (**b**) large scale splitting, (**c**) erosion. The parameters are the same as in Fig. 19, $\gamma = 80$

corresponds rather well to observations of size distributions of marine aggregates in tidal areas [78]. This can be interpreted as a strong hint that large scale splitting might be the dominant fragmentation rule for marine aggregates in coastal waters.

The shape of the size distribution is also dependent on the velocity field of the flow. As long as the attractors for all occurring size classes are space-filling, there are no large qualitative differences between the limiting size distributions. Quantitatively, the differences are due to the shear induced by the flow field. However, if the attractors appearing for different flows are not all space filling but differ essentially with respect to their extension in the configuration space (localised vs. space filling) or dynamically (periodic and quasiperiodic vs. chaotic) then large differences in the steady state size distributions may be found.

7 Future Directions

The ubiquity and relevance of suspended particles in time-dependent flows makes it very important to understand properly the dynamics of finite-size particle advection in chaotic flows. This area is in active development, and the subject is the source of many tantalising questions to scientists. We list below what we think are some promising directions of this field.

Active inertial flows. The existing theory of active flows (that is, the dynamics of chemical reactions or other active processes taking place in a flow) is currently formulated mainly for passive tracers [79]. However, this theory only assumes the existence of fractal spatial distribution of the particles in the flow, and exponential contraction towards these fractal filaments. Generally, in case of inertial particles, as discussed extensively in this paper, the fractal structures are present in a phase space which is higher dimensional than the configuration space. If the projection of the phase space to the configuration space shows a fractal distribution of particles, we can expect that the theory developed for passive tracers holds for inertial particles as well. A major difference, however, is that particles of different size or inertia are expected

to occupy slightly different fractal sets. For example, in the case of species coexistence, a recent work shows that inertia can have a dramatic effect on the population dynamics [80], indicating that it is very important in general active processes. The coagulation and fragmentation process of Sect. 6 is another example of an active process for which the particles' inertia is essential.

Non-spherical particles. Up to now most of the work has been devoted to particles of spherical shape; Eq. (2) is only valid for spherical particles. This approximation works well in case of the formation of raindrops, but is only a rather crude approximation in many other applications like e.g. marine aggregates, which have a fractal-like structure. It can be expected that the non-spherical shape of the particles has a large influence on the dynamics of the particles [81]. As an example the aggregation theory of dust particles in planet formation has been discussed by Wilkinson et al. [68]. While fractal-like particles have been investigated in the context of a mean field approach to describe aggregation and fragmentation [82, 83], the consideration of such non-spherical particles in chaotic flows is a topic of current research.

Hydrodynamical interactions between particles. By moving in the flow, particles modify the velocity field in their vicinity, and this change may in its turn affect the motion of another nearby particle. In this way, a hydrodynamical interaction between particles is created which amounts to an inter-particle force. This effect is usually neglected, but may become very important in high particle concentrations. A particularly important question in this context is how the fractal particle distributions created by chaotic advection are affected by the inter-particle interactions [84].

Non-rigid particles. The Maxey-Riley equation assumes a rigid particle, but there are many important cases where the "particle" is non-rigid. An example is raindrops, or any other liquid droplets within a fluid flow [85]. The fact that their shape is variable and depends in particular on the strain makes their treatment challenging, but important.

Neglected terms in the Maxey-Riley equations. In numerical or analytical investigations of finite-size particles in chaotic flows, the history term and the Faxén terms of the Maxey-Riley equation are almost universally neglected by researchers. It is important to have a more rigorous treatment of these terms [86], and to know more precisely under what conditions one can neglect them, and if there are particular flows for which these terms can be important.

We finish with a brief discussion on the case of particles advected by turbulent flows. We have focused throughout this work on the case of non-turbulent (though chaotic) flows. There is a vast literature on effects of inertia in fully developed turbulence, an important subject for many areas. Today it is possible to investigate the particle properties in turbulence at high spatial and temporal resolution. By the appearance of advanced experimental techniques [87, 88] a direct comparison of experiments and numerical simulations is available. The smallest scales in turbulence are given by the Kolmogorov length $\eta = (\nu^3/\epsilon)^{1/4}$ and the Kolmogorov

time $\tau_\eta = (\nu/\epsilon)^{1/2}$, where ϵ denotes the energy dissipation rate [88]. It is natural to define a Stokes number St_η as the ratio of the Stokesian relaxation time $\tau = 2a^2/(9R\nu)$ following from Eq. (2) for particles of size a to τ_η: $\mathrm{St}_\eta = \tau/\tau_\eta$. Note that this Stokes number differs from the one used throughout the paper which is $\mathrm{St} = \tau U/L$ (as can be seen from (6)), i.e., the ratio of τ to the large scale hydrodynamical time. The particle dynamics in turbulence depends on the scale of observation.

On small scales, below the Kolmogorov lengths (in the so-called dissipative range), the flow is smooth, and viscosity dominates. The overall situation is similar to what has been discussed in the bulk of the paper: particles tend to accumulate on chaotic attractors (projected to the space of the flow), and show fractal patterns. The characteristic dimension (e.g., the Kaplan-Yorke dimension [17]) starts to deviate (quadratically) from the dimension n of the flow as St_η takes on small but positive values [89]. The dimension then reaches a minimum value at a Stokes number $\mathrm{St}_{\eta 1}$ of order one, corresponding to a strongest clustering, also called preferential concentration, with a clean fractal structure. A further increase of the Stokes number leads to an increase of dimension, which reaches again the value of n at some $\mathrm{St}_{\eta 2} > \mathrm{St}_{\eta 1}$, still of order one. Beyond this Stokes number, the attractor dimension is larger than n in the full phase space, and its projection on the fluid is space-filling. This scenario appears to be independent of the Reynolds number of the flow [90] but depends smoothly on the density ratio R [91]. An important observation is that the velocity of the particles as a function of the spatial coordinate might be multivalued. Locations where the multivaluedness starts to develop are called caustics [89, 92, 93] and their existence has serious consequences for collision rates of finite-size particles.

Beyond the Kolmogorov length (in the inertial range), the particle distribution is no longer scale invariant, but it is characterised by voids spanning all scales. Heavy particles have been found to cluster where the acceleration is large, i.e., where pressure gradients dominate [89]. Light particles prefer to stay in regions of the flow characterised by rotation [91]. In the inertial range, preferential concentration appears thus to coincide with regions of certain Eulerian characteristics.

The research of the Lagrangian properties of particles in turbulence is rapidly growing (see the review of [88]), and interesting new insights are likely to emerge. Of particular interest is the behaviour of inertial particles in non-ideal (e.g., not fully developed) turbulence. When a large scale flow is superimposed on ideal turbulence, we expect that the particle dynamics on this scale becomes again similar in nature to that on small scales, and the ideas worked out in the bulk of the paper are then directly applicable.

Acknowledgement U.F. would like to thank Jens C. Zahnow for preparing the figures for Sect. 6. J.H.E.C. and O.P. would like to acknowledge the contributions their colleagues Armando Babiano, Mario Feingold, Marcelo Magnasco, Antonello Provenzale and Idan Tuval have made to their understanding of this subject.

References

1. M. R. Maxey and J. J. Riley. *Equation of motion for a small rigid sphere in a nonuniform flow*. *Phys. Fluids*, **26**, 883 (1983).
2. T. R. Auton, F. C. R. Hunt, and M. Prud'homme. *The force exerted on a body in inviscid unsteady non-uniform ratational flow*. *J. Fluid. Mech.*, **197**, 241 (1988).
3. G. I. Taylor. *The forces on a body placed in a curved or converging stream of fluid*. *Proc. R. Soc. London A*, **120**, 260 (1928).
4. H. Aref. *Stirring by chaotic advection*. *J. Fluid Mech.*, **143**, 1 (1984).
5. J. M. Ottino. *The Kinematics of Mixing: Stretching, Chaos and Transport*. Cambridge University Press, Cambridge (1989).
6. H. Aref. *Chaos Applied to Fluid Mixing*. Pergamon Press, Oxford (1995).
7. E. E. Michaelides. *The transient equation of motion for particles, bubbles, and droplets*. *J.Fluids Eng.*, **119**, 233 (1997).
8. J. Magnudet and I. Eames. *The motion of high-Reynolds-number bubbles in inhomogeneous flows*. *Annu. Rev. Fluid. Mech.*, **32**, 659 (2000).
9. E. E. Michaelides. *Particles, Bubbles and Drops: Their Motion, Heat and Mass Transfer*. World Scientific, Singapore (2006).
10. A. B. Basset. *On the motion of a sphere in a viscous liquid*. *Phil. Trans. Roy. Soc*., **179**, 43 (1888).
11. J. Boussinesq. *Sur la résistance qu'oppose un fluide indéfini en repos, sans pesanteur, au mouvement varié d'une sphère solide qu'il mouille sur toute sa surface, quand les vitesses restent bien continues et assez faibles pour que leurs carrés et produits soient négligeables*. *C. R. Acad. Sci. Paris*, **100**, 935 (1885).
12. M. R. Maxey. *The gravitational settling of aerosol-particles in homogeneous turbulence and random flow-fields*. *J. Fluid. Mech.*, **174**, 441 (1987).
13. J. J. B. Biemond et al. *Onset of chaotic advection in open flows*. *Phys. Rev. E*, **78**, 016317 (2008).
14. M. Van Dyke. *An Album of Fluid Motion*. Parabolic Press, Stanford (1982).
15. J. C. Sommerer et al. *Experimental evidence for chaotic scattering in a fluid wake*. *Phys. Rev. Lett.*, **77**, 5055 (1996).
16. J. H. E. Cartwright, M. Feingold, and O. Piro. "An introduction to chaotic advection." In H. Chate, E. Villermaux, and J. M. Chomez, editors, *Mixing: Chaos and Turbulence*. Kluwer, Dordrecht, pp. 307–342 (1999).
17. L. D. Landau and E. M. Lifshits. *Fluid Mechanics*. Elsevier, Butterworth-Heinemann, Oxford, UK (2000).
18. G. K. Batchelor. *An Introduction to Fluid Dynamics*. Cambridge University Press, Cambridge (1967).
19. E. Ott. *Chaos in Dynamical Systems*. Cambridge University Press, Cambdridge (2002).
20. T. Tél and M. Gruiz. *Chaotic Dynamics*. Cambridge University Press, Cambridge (2006).
21. S. Chadrasekhar. *Hydrodynamic and Hydromagnetic Stability*. Oxford University Press, Oxford (1961).
22. S. Wiggins. *Global Bifurcations and Chaos*. Springer, New York (1988).
23. T. Nishikawa et al. *Finite-size effects on active chaotic advection*. *Phys. Rev. E*, **65**, 026216 (2002).
24. P. K. Kundu. *Fluid Mechanics*. Academic Press, New York (1990).
25. C. Jung, T. Tél, and E. Ziemniak. *Application of scattering chaos to particle transport in a hydrodynamical flow*. *Chaos*, **3**, 555 (1993).
26. E. Ziemniak, C. Jung, and T. Tél. *Tracer dynamics in open hydrodynamical flows as chaotic scattering*. *Phys. D*, **79**, 424 (1994).
27. C. Jung and E. Ziemniak. *Hamiltonian scattering chaos in a hydrodynamical system*. *J. Phys. A*, **25**, 3929 (1992).

28. Á. Péntek, Z. Toroczkai, T. Tél, C. Grebogi, and Y. Yorke. *Fractal boundaries in open hydrodynamical flows – signatures of chaotic saddles*. *Phys. Rev. E*, 51, 4076 (1995).
29. M. A. Sanjuán, J. Kennedy, E. Ott, and J. A. Yorke. *Indecomposable continua and the characterization of strange sets in nonlinear dynamics*. *Phys. Rev. Lett.*, **78**, 1892 (1997).
30. M. A. F. Sanjuan, J. A. Kennedy, C. Grebogi, and J. A. Yorke. *Indecomposable continua in dynamical systems with noise: Fluid flow past an array of cylinders*. *Chaos*, **7** 125 (1997).
31. I. Scheuring, T. Czárán, P. Szabó, G. Károlyi, and Z. Toroczkai. *Spatial models of prebiotic evolution: soup before pizza? Orig. Life Evol. Biosph.*, **33**, 319 (2003).
32. M. Sandulescu, E. Hernandez-Garcia, C. López, and U. Feudel. *Kinematic studies of transport across an island wake, with application to the Canary islands*. *Tellus A*, **58**, 605 (2007).
33. M. Sandulescu, C. E. López, E. Hernandez-Garcia, and U. Feudel. *Plankton blooms in vortices: the role of biological and hydrodynamic timescales*. *Nonlinear Proc. Geophys.*, **14**, 1 (2007).
34. O. A. Druzhinin and L. A. Ostrovsky. *The influence of Basset force on particle dynamics in 2-dimensional flows*. *Phys. D*, **76**, 34 (1994).
35. P. Tanga and A. Provenzale. *Dynamics of advected tracers with varying buoyancy*. *Phys. D*, **76**, 202 (1994).
36. A. N. Yannacopoulos, G. Rowlands, and G. P. King. *Influence of particle inertia and Basset force on tracer dynamics: Analytic results in the small-inertia limit*. *Phys. Rev. E*, **55**, 4148 (1997).
37. J. R. Angilella. *Asymptotic analysis of chaotic particle sedimentation and trapping in the vicinity of a vertical upward streamline*. *Phys. Fluids*, **19**, 073302 (2007).
38. J. R. Angilella. *Chaotic particle sedimentation in a rotating flow with time-periodic strength*. *Phys. Rev. E*, **78**, 066310 (2008).
39. F. Candelier, J. R. Angilella, and M. Souhar. *On the effect of the Boussinesq-Basset force on the radial migration of a Stokes particle in a vortex*. *Phys. Fluids*, **16**, 1765 (2004).
40. F. Candelier and J. R. Angilella. *Analytical investigation of the combined effect of fluid inertia and unsteadiness on low-Re particle centrifugation*. *Phys. Rev. E*, **73**, 047301 (2006).
41. A. Babiano, J. H. E. Cartwright, O. Piro, and A. Provenzale. *Dynamics of a small neutrally buoyant sphere in a fluid and targeting in Hamiltonian systems*. *Phys. Rev. Lett.,* **84**, 5764–5767 (2000).
42. A. Crisanti, M. Falcioni, A. Provenzale, and A. Vulpiani. *Passive advection of particles denser than the surrounding fluid*. *Phys. Lett. A*, **150**, 79 (1990).
43. A. Okubo. *Horizontal dispersion of floatable particles in vicinity of velocity singularities such as convergences*. *Deep-Sea Res.*, **17**, 445 (1970).
44. J. B. Weiss. *The dynamics of enstrophy transfer in 2-dimensional hydrodynamics*. *Phys. D*, **48**, 273 (1991).
45. D. Elhmaidi, A. Provenzale, and A. Babiano. *Elementary topology of 2-dimensional turbulence from a Lagrangian viewpoint and single-particle dispersion*. *J. Fluid Mech.*, **257**, 533 (1993).
46. C. Basdevant and T. Philipovich. *On the validity of the Weiss criterion in 2-dimensional turbulence*. *Phys. D*, **73**, 17 (1994).
47. B. L. Hua and P. Klein. *An exact criterion for the stirring properties of nearly two-dimensional turbulence*. *Phys. D*, **113**, 98 (1998).
48. B. Protas, A. Babiano, and N. K.-R. Kevlahan. *On geometrical alignment properties of two-dimensional forced turbulence*. *Phys. D*, **128**, 169 (1999).
49. A. Provenzale. *Transport by coherent barotropic vortices*. *Annu. Rev. Fluid Mech.*, **31**, 55 (1999).
50. G. Haller and T. Sapsis. *Where do inertial particles go in fluid flows? Phys. D*, **237**, 573 (2008).
51. T. Sapsis and G. Haller. *Instabilities in the dynamics of neutrally buoyant particles*. *Phys. Fluids*, **20**, 017102 (2008).
52. J. H. E. Cartwright, M. O. Magnasco, and O. Piro. *Bailout embeddings, targeting of invariant tori, and the control of Hamiltonian chaos*. *Phys. Rev. E*, **65**, 045203(R) (2002); J. H. E.

Cartwright, M. O. Magnasco, O. Piro, and I. Tuval. *Bailout embeddings and neutrally buoyant particles in three-dimensional flows*. *Phys. Rev. Lett.*, **89**, 264501 (2002); J. H. E. Cartwright, M. O. Magnasco, O. Piro, and I. Tuval. *Noise-induced order out of chaos by bailout embedding*. *Fluctuation Noise Lett.*, **2**, 161 (2002); J. H. E. Cartwright, M. O. Magnasco, O. Piro, and I. Tuval. *Bubbling and on-off intermittency in bailout embeddings*. *Phys. Rev. E*, **68**, 016217 (2003).

53. J. H. E. Cartwright, M. O. Magnasco, O. Piro, and I. Tuval. *Noise- and inertia-induced inhomogeneity in the distribution of small particles in fluid flows*. *Chaos*, **12**, 489 (2002).
54. V. I. Arnold. *Sur la topologie des écoulements stationnaires des fluides parfaits*. *C. R. Acad. Sci. Paris A*, **261**, 17 (1965); M. Hénon. *Sur la topologie des lignes de courant dans un cas particulier*. *C. R. Acad. Sci. Paris A*, **262**, 312 (1966).
55. T. Dombre et al. *Chaotic streamlines in the ABC flows*. *J. Fluid Mech.*, **167**, 353 (1986).
56. I. J. Benczik, Z. Toroczkai, and T. Tél. *Selective sensitivity of open chaotic flows on inertial tracer advection: Catching particles with a stick*. *Phys. Rev. Lett.*, **89**, 164501 (2002).
57. I. Benczik, T. Toroczkai, and T. Tél. *Advection of finite-size particles in open flows*. *Phys. Rev. E*, **67**, 036303 (2003).
58. Y. Do and Y.-C. Lai. *Superpersistent chaotic transients in physical space: advective dynamics of inertial particles in open chaotic flows under noise*. *Phys. Rev. Lett.*, **91**, 224101 (2003).
59. G. Haller and T. Sapsis. *Localized instability and attraction along invariant manifolds*. (2009).
60. W. Tang, G. Haller, J.-J. Baik, and Y.-H. Tyu. *Locating an atmospheric contamination source using slow manifolds*. *Phys. Fluids*, **21**, 043302 (2009).
61. T. Sapsis and G. Haller. Inertial particle dynamics in a hurricane. *J. Atmos. Sci.*, **66**, 2481–2492 (2009).
62. R. D. Vilela and A. E. Motter. *Can aerosols be trapped in open flows? Phys. Rev. Lett.*, **99**, 264101 (2007).
63. R. D. Vilela, A. P. S. de Moura, and C. Grebogi. *Finite-size effects on open chaotic advection*. *Phys. Rev. E*, **73**, 026302 (2006).
64. H. R. Pruppacher and J. D. Klett. *Microphysics of Clouds and Precipitation*. Kluwer Academic Publishers, Dordrecht (1997).
65. G. A. Jackson. *A model of the formation of marine algal flocs by physical coagulation processes*. *Deep-Sea Res.*, **37**, 1197 (1990).
66. W. McAnally and A. Mehta. *Significance of aggregation of fine sediment particles in their deposition*. *Estuarine Coastal Shelf Sci.*, **54**, 643 (2002).
67. C. Crowe, M. Sommerfeld, and Y. Tsuji. *Multiphase Flows with Particles and Droplets*. CRC Press, New York (1998).
68. M. Wilkinson et al. *Stokes trapping and planet formation*. *Astrophys. J. Suppl. Ser.*, **176**, 484 (2008).
69. J. Zhang and X.-Y. Li. *Modeling particle-size distribution dynamics in a flocculation system*. *AIChE J.*, **49**, 1870 (2003).
70. J. C. Zahnow and U. Feudel. *Moving finite-size particles in a flow: A physical example of pitchfork bifurcations of tori*. *Phys. Rev. E*, **77**, 026215 (2008).
71. T. Nishikawa et al. *Advective coalescence in chaotic flows*. *Phys. Rev. Lett.*, **87**, 038301 (2001).
72. J. C. Zahnow, R. D. Vilela, U. Feudel et al. *Coagulation and fragmentation dynamics of inertial particles*. *Phys. Rev. E*, **80**, 026311 (2009).
73. E. Villermaux. *Fragmentation*. *Annu. Rev. Fluid Mech.*, **39**, 419 (2007).
74. A. Alldredge et al. *The physical strength of marine snow and its implications for particle disaggregation in the ocean*. *Limnol. Oceanogr.*, 35,1415 (1990).
75. G. I. Taylor. *The formation of emulsions in definable fields of flow*. *Proc. Roy. Soc. A*, **146**, 501 (1934).
76. M. Delichatsios. *Model for breakup rate of spherical drops in isotropic turbulent flows*. *Phys. Fluids*, **30**, 622 (1975).
77. J. C. Zahnow et al. *Aggregation and fragmentation dynamics of inertial particles in chaotic flows*. *Phys. Rev. E*, **77**, 055301(R) (2008).

78. M. Lunau et al. *Physical and biogeochemical controls of microaggregate dynamics in a tidally affected coastal ecosystem*. *Limnol. Oceanogr.*, **51**, 847 (2006).
79. Z. Toroczkai, G. Károlyi, A. Péntek, T. Tél, and C. Grebogi. *Advection of active particles in open chaotic flows*. *Phys. Rev. Lett.*, **80**, 500 (1998); T. Tél, A. P. S. de Moura, G. Károlyi, and C. Grebogi. *Chemical and biological activity in open flows: A dynamical system approach*. *Phys. Rep.*, 413, 91 (2005); J. H. E. Cartwright, J. M. Garcia-Ruiz, O.Piro, C. I. Sainz-Diaz, and I. Tuval. *Chiral symmetry breaking during crystallization: An advection-mediated nonlinear auto- catalytic process. Phys. Rev. Lett.* **93**, 035502 (2004); J. H. E. Cartwright, O.Piro, and I. Tuval. *Ostwald ripening, chiral crystallization, and the common-ancestor effect. Phys. Rev. Lett.,* **98**, 165501 (2007).
80. I. J. Benczik, G. Károlyi, I. Scheuring, and T. Tél. *Coexistence of inertial competitors in chaotic flows*. *Chaos*, **16**, 043110 (2006).
81. H. Shin and M. R. Maxey. *Chaotic motion of nonspherical particles settling in a cellular flow field*. *Phys. Rev. E*, **56**, 5431 (1997).
82. C. Kranenburg. *The fractal structure of cohesive sediment aggregates*. *Estuarine Coastal Shelf Sci.*, **39**, 541 (1994).
83. F. Maggi, F. Mietta, and J. C. Winterwerp. *Effect of variable fractal dimension on the floc size distribution of suspended cohesive sediment*. *J. Hydrol.*, **343**, 43 (2007).
84. R. Medrano, A. Moura, T. Tel, I. Caldas, and C. Grebogi. *Finite-size particles, advection, and chaos: A collective phenomenon of intermittent bursting*. *Phys. Rev. E,* **78**, 56206 (2008).
85. M. Tjahjadi and J. M. Ottino. *Stretching and breakup of droplets in chaotic flows*. *J. Fluid Mech.,* **232**, 191 (1991); J. M. Ottino. *Unity and diversity in mixing: Stretching, diffusion, breakup, and aggregation in chaotic flows. Phys. Fluids A*, **3**, 1417 (1991).
86. N. Mordant and J. -F. Pinton. *Velocity measurement of a settling sphere*. *Eur. Phys. J.* **B 18**, 343–352 (2000).
87. N. T. Ouellette, P. J. O'Malley, and J. P. Gollub. *Transport of finite-sized particles in chaotic flow*. *Phys. Rev. Lett.*, **101**, 174504 (2008).
88. F. Toschi and E. Bodenschatz. *Lagrangian properties of particles in turbulence*. *Annu. Rev. Fluid. Mech.*, **41**, 375 (2009).
89. J. Bec. *Fractal clustering of inertial particles in random flows*. *Phys. Fluids*, **15**, L81 (2003).
90. J. Bec et al. *Heavy particle concentration in turbulence at dissipative and inertial scales*. *Phys. Rev. Lett.*, **98**, 084502 (2008).
91. E. Calzavarini, M. Kerscher, D. Lohse, and F. Toschi. *Dimensionality and morphology of particle and bubble clusters in turbulent flow*. *J. Fluid Mech.*, **607**, 13 (2008).
92. G. Falkovich, A. Fouxon, and M. G. Stepanov. *Acceleration of rain initiation by cloud turbulence*. *Nature*, **419**, 151 (2002).
93. M. Wilkinson and B. Mehlig. *Caustics in turbulent aerosols*. *Europhys. Lett.*, **71**, 186 (2005).
94. H. Faxén. *Der Widerstand gegen die Bewegung einer starren Kugel in einer zähen Flüssigkeit, die zwischen zwei parallelen ebenen Wänden eingeschlossen ist*. *Ann. Phys.*, **4**, 89 (1922).